Selective deletion of *Caspase-3* gene in the dopaminergic system exhibits autistic-like behaviour

Irene García-Domínguez[1#], Irene Suárez-Pereira[2#], Marti Santiago[1], Eva M. Pérez-Villegas[3], Lidia Bravo[2], Carolina López-Martín[2], María Angustias Roca-Ceballos[1], Juan García-Revilla[1], Ana M. Espinosa-Oliva[1], José A. Rodríguez-Gómez[1,4], Bertrand Joseph[5], Esther Berrocoso[2], José Ángel Armengol[3], José L. Venero[1ψ], Rocío Ruiz[1ψ*], Rocío M. de Pablos[1ψ]

[1]Departamento de Bioquímica y Biología Molecular, Facultad de Farmacia, Universidad de Sevilla, and Instituto de Biomedicina de Sevilla-Hospital Universitario Virgen del Rocío/CSIC/Universidad de Sevilla, Sevilla, Spain.

[2]Centro de Investigación Biomédica en Red de Salud Mental (CIBERSAM), Instituto de Salud Carlos III, Spain; Neuropsychopharmacology & Psychobiology Research Group, University of Cádiz, Spain; Instituto de Investigación e Innovación en Ciencias Biomédicas de Cádiz, INiBICA, Edificio "Andrés Segovia", Cádiz, Spain.

[3]Departamento de Fisiología, Anatomía y Biología Celular, Universidad Pablo de Olavide, Sevilla, Spain.

[4]Departament of Medical Physiology and Biophysics, Faculty of Medicine, University of Seville, 41009 Sevilla, Spain and Instituto de Biomedicina de Sevilla-Hospital Universitario Virgen del Rocío/CSIC/Universidad de Sevilla, Sevilla, Spain.

[5]Institute of Environmental Medicine, Toxicology Unit, Karolinska Institutet, Stockholm, Sweden.

[#]Irene García-Domínguez and Irene Suárez-Pereira shared first authorship.

[ψ]José Luis Venero, Rocío Ruiz and Rocío M. de Pablos shared senior authorship.

***Corresponding author:** Rocío Ruiz, Ph.D. Departamento de Bioquímica y Biología Molecular, Facultad de Farmacia, Universidad de Sevilla, and Instituto de Biomedicina de Sevilla-Hospital Universitario Virgen del Rocío/CSIC/Universidad de Sevilla, Sevilla, Spain. Phone: +34-954-556756, e-mail: rruizlaza@us.es. http://orcid.org/0000-0001-5142-9972.

ABSTRACT

Apoptotic caspases are thought to play critical roles in elimination of excessive and non-functional synapses and removal of extra cells during early developmental stages. Hence, an impairment of this process may thus constitute a basis for numerous neurological and psychiatric diseases. This view is especially relevant for dopamine due to its pleiotropic roles in motor control, motivation and reward processing. Here, we have analysed the effect of caspase-3 depletion on the development of catecholaminergic neurons and performed a wide array of neurochemical, ultrastructural and behavioural assays. To achieve this, we performed selective deletion of the *Casp3* gene in tyrosine hydroxylase (TH)-expressing cells using Cre-loxP-mediated recombination. Histological evaluation of most relevant catecholaminergic nuclei revealed the ventral mesencephalon as the most affected region. Stereological analysis demonstrated an increase in the number of TH-positive neurons in both the substantia nigra and ventral tegmental area along with enlarged volume of the ventral midbrain. Analysis of main innervating tissues revealed a rather contrasting profile. In striatum, basal extracellular levels and potassium-evoked DA release were significantly reduced in mice lacking *Casp3*, a clear indication of dopaminergic hypofunction in dopaminergic innervating tissues. This view was sustained by analysis of TH-labeled dopaminergic terminals by confocal and electron microscopy. Remarkably, at a behavioural level, C*asp3*-deficient mice exhibited impaired social interaction, restrictive interests and repetitive stereotypies, which are considered the core symptoms of autism spectrum disorder (ASD). Our study revitalizes the potential involvement of dopaminergic transmission in ASD and provides an excellent model to get further insights in ASD pathogenesis.

KEYWORDS: Caspase, autisms, dopaminergic system, catecholaminergic neurons, tyrosine hydroxylase

INTRODUCTION

Autism spectrum disorder (ASD) is a highly prevalent, lifelong heterogeneous neurodevelopmental disorder present from early childhood. ASD is among the most common developmental neuropsychiatric disorders, affecting 1~2% of the population (Elsabbagh et al., 2012; Kim et al., 2011; Kuo and Liu, 2018). ASD individuals share the core symptoms of unusual reciprocal social interactions and social communication deficits, and stereotyped repetitive behaviour with restricted interests and activities (Vahia, 2013). In addition to the core symptoms, more than 70% of ASD patients also show various physiological and psychiatric comorbid symptoms, including anxiety, intellectual disability, motor abnormalities, epilepsy, seizures, attention and language deficits, hyper or hyporeactivity, sleep disturbance, and gastrointestinal problems (Lai et al., 2014). All these features make of ASD a disorder that imposes a significant social-economic burden. Regrettably, an effective treatment to palliate the core symptoms of ASD is still lacking, being a promising field that needs more research.

Although maternal exposure during pregnancy to different factors (such as infection, ethanol and anti-epileptic drugs) could play a significant role in its aetiology (Arndt et al., 2005), ASD is also a highly heritable disorder (Abrahams and Geschwind, 2008). Whole-exome sequencing of families from the Simons Simplex Collection enabled the identification of about 120 candidate genes associated with ASD. These include some polymorphisms of genes related to the dopaminergic system, such as the D3 and D4 dopamine receptors (*DR3* and *DR4*) and the dopamine transporter *DAT* (Kuo and Liu, 2018). Recently, a single-cell genomic study has identified type-specific molecular changes in ASD, including genes important for synaptic function as well as transcription factors (Velmeshev et al., 2019).

Several hypothesis try to explain ASD pathogenesis, including excitatory/inhibitory imbalance, neurotransmitters dysfunction, dysfunction of the mTOR and the endocannabinoid signalling pathways, as well as neuroinflammation and epigenetic alterations (Kuo and Liu, 2018). Despite this, the pathogenesis of ASD remains largely unknown. In this regard, accumulating evidence suggest that ASD might be linked to dopaminergic dysfunctions (Dichter et al., 2012b; Ernst et al., 1997; Lee et al., 2018; Pavăl, 2017; Scott-Van Zeeland et al., 2010). Early evidence pointing to catecholamine dysfunction in ASD patients was based on the finding that there were increased levels of norepinephrine and decreased levels of dopamine-β-hydroxylase -the enzyme that converts dopamine (DA) to norepinephrine- activity in the plasma of these patients (Lake et al., 1977). Since these observations, numerous authors have put forth the idea that DA imbalance in specific brain regions could lead to autistic-like behaviour (Dichter et al., 2012a). Therefore, it has been hypothesized that a dysfunction of the mesocorticolimbic circuit leads to social deficits, while a dysfunction of the nigrostriatal circuit leads to stereotyped behaviours;

both considered the main symptoms of ASD. However, existing views fail to clarify the role of DA signalling anomalies in prompting the behavioural features of ASD. Thus, despite extensive research into the matter, a demonstration of the DA hypothesis of ASD is currently lacking. Therefore, the development of a dopaminergic animal model of ASD is mandatory for linking neurobiology to behaviour; this link would be a first step that would allow a better understanding of the ASD pathogenesis.

Caspase-3 (CASP3) is a cysteine-aspartic acid protease that plays a central role in the execution-phase of apoptosis. However, in recent years, several groups have demonstrated that CASP3 has many other non-apoptotic functions in a multitude of cellular processes, including inflammation, cell differentiation and proliferation (Burguillos et al., 2011). In the CNS, CASP3 plays non-apoptotic roles in synaptic plasticity (Li et al., 2010), pruning (Kuo et al., 2006; Williams et al., 2006) and neurite growth (Westphal et al., 2010). Its key role in neurodevelopment has been demonstrated by the important defects observed in the brain of mice deficient in this protease (*Casp3*$^{-/-}$) (Kuida et al., 1996). Moreover, the participation of CASP3 in the physiological death regulating the number of dopaminergic midbrain neurons during development has also been demonstrated (Jeon et al., 1999). All these data clearly establish the importance of this protease in embryonic neuronal development.

Here, we provide a novel ASD model based on the selective deletion of *Casp3* in tyrosine hydroxylase (TH)-expressing neurons using the TH-IRES-Cre mouse. Taking into account the importance of this caspase in the development of the dopaminergic system (Jackson-Lewis et al., 2000; Zhang et al., 2007), here we demonstrate that selective deletion of *Casp3* in TH-expressing cells confers dopaminergic hyperinnervation in the ventral mesencephalon and striatal DA hypofunction with abnormal motor behaviour. Unexpectedly, these mice exhibited a prominent autistic-like behaviour including social interaction, communication impairment and stereotypies thus rising as a promising ASD animal model. Furthermore, these mice offer a unique model to study the possible implication of DA in the pathogenesis of ASD.

MATERIAL AND METHODS

Animal Model

Caspase-3$^{f/f}$ C57BL/6 mice with the CASP3 allele floxed at exon 2 were generously provided by Prof. Richard Flavell (Yale University). C57BL/6 mice containing a IRES-Cre recombinase under the control of TH promoter were kindly provided by José I. Piruat (Instituto de Biomedicina de Sevilla). Both colonies were maintained at the Centre of Production and Animal Experimentation of the University of Seville. Animals were housed at constant room temperature (RT) of 22 ± 1º C and relative humidity (60%), with a 12-h light-dark cycle and *ad*

libitum access to food and water. Experiments were carried out in accordance with the Guidelines of the European Union Directive (2010/63/EU) and Spanish regulations (BOE 34/11370-421, 2013) for the use of laboratory animals; the study was approved by the Scientific Committee of the University of Seville.

In our experimental conditions, the *Cre* gene is preceded by encephalomyocarditis virus IRES by a knock-in strategy (Lindeberg et al., 2004). This enables expression of bicistronic mRNA encoding both TH and Cre (Lindeberg et al., 2004). This strategy has provided very efficient genomic recombination in TH-expressing cells. However, germ cells of both sexes were also shown to exhibit recombination. This feature was used as a novel strategy to knock out *Caspase-3* in one allele by crossing $TH^{Cre}CASP3^{f/wt}$ with $CASP3^{f/f}$ to generate $TH^{Cre}CASP3^{f/-}$ mice (experimental mouse, hereinafter TH-CASP3KO). This strategy ensures high deletion of the *Casp3* gene in TH-expressing cells (Fig. 1A). Three to six month-old male TH-CASP3KO and C57BL/6 mice (control) (20-25 g) were used in our experiments.

Behavioural testing

Behavioural experiments were conducted in dedicated behavioural testing rooms during the standard light phase, usually between 09:00 and 15:00 h. Mice were brought to a holding room in the hallway of the testing area at least 30 min prior to behavioural testing. All task equips were cleaned thoroughly with 70% ethanol between trials to remove any olfactory cues. Fully blind rating in tasks that were scored in real time, as well as when scoring was conducted from videotaped sessions. At least 6 mice per genotype were tested on all behavioural assays. Additional mice underwent behavioural testing on more than one, but not all assays. Each animal performed different behavioural tests, but not all of the proposals, always allowing them a rest between tests and establishing an ascending stress testing order. So, the following testing order was used in two independent experimental rounds: 1/ locomotor activity/open field, marble buried, rotarod, tail suspension test and prepulse inhibition of acoustic startle response; 2/ nesting, olfatory test, hot plate, social behavior and motor activity in response to amphetamine. Experimental mice derived from four different litters in the first round of experiments. Four additional litters were used in the second round of experiments.

Locomotor activity: Spontaneous activity was measured during 30 min (Ramos-Rodriguez et al., 2013). Mice were placed in a square arena (45 x 45 cm) enclosed by continuous, 35-cm-high, opaque walls, located in a room with constant dim lighting (estimated about 10 to 20 lux) and with constant background noise (i.e. the behavioural tests were performed in silence, avoiding making noise except for the unavoidable room background noise, such as the ventilation or light system). All sessions were recorded and evaluated using the SMART 3.0 video tracking system (Panlab). Activity in arbitrary units (mobility respect to reference, video

snapshot, by the software) was collected in 5 min intervals and total time. In addition, the resting time and the number of grooming and rearing events were registered as a measure of motor stereotypies.

Open field (OF): The open field test was performed in 2,025 cm^2 enclosure over 10 min, the centre of which was defined as a square that covered 50% of the total OF square area. The time spent in the central area was monitored over a 10 min test period using the SMART 3.0 video tracking system (Panlab). Thigmotactic behaviour data are expressed as Log of the ratio ($time_{margin}/time_{centre}$) (Wurzman et al., 2015). In addition, the number of fecal boluses was recorded manually as a measure of anxiety.

Rotarod: Motor coordination and balance were evaluated in a rotarod apparatus (Panlab). Mice were placed on the rotarod and were performed two test: at a constant speed (5 rpm) for a maximum of 5 min (3 trials with 15 min rest between trials), and at accelerated speed (4 to 40 rpm in 5 min, only 1 trial) (Nóbrega et al., 2013). Number of falls was counted by the researcher and the latency to fall was automatically recorded by the apparatus, respectively.

Marble buried: Mice were placed in a standard plastic cage (40 x 24 x 18 cm) without a lid but with a filter top so that mice could not cling to the cage lid and could not escape (Wurzman et al., 2015). The cage contained 20 glass marbles evenly spaced (5 rows of 4 marbles per row) on top of 4.5 cm of bedding. After 30 min the mouse was removed and the number of buried marbles (>2/3rds covered) was counted.

Tail suspension test (TST): Mice were individually and securely suspended during 6 min by the distal end of the tail from an aluminium hook raised 20 cm above the floor using adhesive tape. The test sessions were recorded and analyzed blindly by a researcher (Berrocoso et al., 2013). The analysis procedure used was a time sampling technique, whereby the predominant behaviour in each 5-s period of the 360 s test was scored. The behaviours rated were: (1) immobility – a mouse was judged to be immobile when it hung by its tail without engaging in any active behaviour; (2) swinging – a mouse was judged to be swinging when it continuously moved its paws in the vertical position while keeping its body straight and/or it moved its body from side to side; (3) curling – a mouse was judged to be curling when it engaged in active twisting movements of the entire body; (4) clasping – a mouse was judged to be clasping when it showed hindlimb grasping behaviour towards the abdomen.

Prepulse inhibition (PPI) of acoustic startle response (ASR): Mice were tested for ASR and PPI using the startle reflex system (Panlab) (Urigüen et al., 2013). Background noise (65 dB) was present throughout the session. The startling stimulus was a broadband acoustic pulse with an intensity of 120 dB and duration of 30 milliseconds (ms), and was either administered alone

("pulse-alone" trials) or paired with the prior presentation of 30 ms duration prepulse ("prepulse" trials). The prepulse stimulus intensity was set to 3, 6, or 12 dB above background noise and was delivered with an interstimulus interval of 120 ms (onset-to-onset). A testing session contained a habituation period, a baseline with 5 pulse-alone, a total of 40 test-trials (10 pulse-alone and 10 prepulse trials at each prepulse intensity) and a final repetition of baseline. Inter-trial intervals ranged from 10-20 s. Startle magnitude was calculated as the average of the startle responses to the respective pulse trials. PPI was calculated according to the formula: %PPI = (1 - (startle response for prepulse + pulse trials/startle response for pulse alone trials)) × 100.

Olfatory test: Mice were habituated to the flavour of a novel food (Kellogg's Chocolate Cereal bar) for 3 days prior, in order to avoid food neophobia on the day of testing. Olfactory ability was evaluated following a period of food deprivation; all food was removed from the home cage 16–20 h before the test. On the day of the test, each mouse was placed in a clean cage containing 3 cm of bedding and allowed to explore for 5 min. The animal was removed from the cage, and 1 cm^3 piece of cereal bar was buried in the cage bedding, approximately 1 cm below the surface of the litter (Moy et al., 2007). The latency to find the food was measured.

Hot plate: Response to an acute thermal stimulus was measured using the hot plate test (Berrocoso and Mico, 2009). The mouse was placed on a flat, black metal surface (Ugo Basile, Socrel DS-37) maintained at 55° C and surrounded by a square transparent plexiglass barrier to prevent jumping off. The latency to the first paw lick, jump or vocalization was measured by an observer using a foot pedal-controlled timer. A maximum cut-off time of 30 s was used to prevent the risk of tissue damage to the paws.

Social behaviour: This experiment was performed in an experimental cage (40 x 24 x 18 cm) with bedding. For habituation, subject mice were first placed in the middle of the cage and allowed to explore for 10 min. For the novelty preference test, an empty wire cage (wire cups; diameter, 7.7 cm; height, 10 cm) was placed in a chamber side, and then the subject mice were allowed to explore for 10 min. For the sociability test, a novel mouse (stranger, different strain, age-matched male C3H/HeJ mice) was enclosed in the wire cage and placed in the same chamber side, and again the subject mice were allowed to explore for 10 min. The time spent in sniffing each wire cage (empty and stranger house) and in each of the side chambers and the latency to the first contact was measured. A mouse was considered to be sniffing the wire cage when its head was facing the cage within 1 cm (Moretti et al., 2005).

Nesting: Nest building and utilization were assessed during 2 days of single housing (Moretti et al., 2005). Nesting material, two cotton wafers (5 cm^3), was introduced in the cage. After 1 h and 24 h, the quality together with the height of the nest was recorded. Nest quality was

measured using the following scale: (0) nesting material unmodified; (1) flat nest with partially shredded nesting material; (2) shallow nest with shredded material, but lacking fully formed walls; (3) nest with well-developed walls; and (4) nest in a shape of a cocoon with partial or complete roof.

Motor activity in response to amphetamine: Amphetamine-induced behavioural sensitization was measured (Urigüen et al., 2013). Mice were injected with amphetamine (5 mg/kg, i.p.) and spontaneous locomotion was evaluated with a computerized video-tracking system (SMART 3.0, PanLab) for 20 min before and 60 min after injection.

Immunohistochemistry

Animals were perfused with paraformaldehyde (4%) at the end of the behavioural experiments. TH expression was evaluated in dopaminergic (substantia nigra (SN), ventral tegmental area (VTA), caudate putamen (CPu)) and noradrenergic nuclei (A1, A2, C1, C2, C3, A5, A6 (LC) and A7). Sections were submitted to an inactivation of endogenous peroxidase with PBS containing 0.3% hydrogen peroxide (30 min) prior to the incubation with a rabbit anti-TH at 4º C (1:1000, Abcam, ab113, for 48 h for optical analysis; 1:2000, Sigma, T8780, for 24 h, for stereological analysis). Subsequently, the sections were incubated 1.5 h with a biotinylated donkey anti-rabbit (1:200, Jackson Immunoresearch Europe, 711-065-152, for optical analysis) or goat anti-rabbit (1:200, Vector, BA-1000, for stereological analysis). Afterwards, sections were incubated for another hour in avidin–biotin complex (ABC, Vector PK-6100) conjugated with horseradish peroxidase (1:200). Visualization of the immunostaining was achieved using the 3,3'-diaminobenzidine tetrahydrochloride (DAB) reaction (5 min in 0.05 M Tris buffer containing 0.05% DAB and 0.003% hydrogen peroxide). Sections were mounted on gelatine-coated slides, cleared in xylene and coverslipped with Eukitt.

For optical density analysis, for each structure, 1 of every 4 sections of 50 µm was evaluated. The number of TH-immunoreactivity (TH-IR) cells was captured on an Olympus BX60 microscope. An experimenter blind to the conditions manually counted the labelled cell bodies (TH-IR) in an average of 4-6 sections per animal (n=4-5). Optical density of TH expression was calculated after delimited the region of interest manually and applying the mean of intensity less the background noise of each section (4-6 sections except for CPu: 10 sections) using Fiji Image J (W. Rasband, National Institutes of Health) and therefore expressing in arbitrary units (a.u.).

For stereological analysis, sections of 30 µm thickness were evaluated. Analysis were made in a bounded region of the SN with a length of 300 microns in the anterior–posterior axis centred at the point of injection (5.5 mm with respect to bregma), that is, between 5.35 and 5.65 mm with respect to bregma (Franklin, 2019). In each case, 5 sections per animal were used, with random

starting point and systematically distributed through the anterior–posterior axis of the analyzed region. The number of TH-positive neurons in the SN was estimated using a fractionator sampling design (Gundersen et al., 1988). Counts were made at regular predetermined intervals (x = 150 µm and y = 200 µm) within each section. An unbiased counting frame of known area (40 µm × 25 µm = 1000 μm^2) was superimposed on the tissue section image under a 100x oil immersion objective. Therefore, the area sampling fraction is 1000/(150 × 200) = 0.033. The entire z-dimension of each section was sampled; hence, the section thickness sampling fraction was 1. In all animals, 30-µm sections, each 100 µm apart, were analysed; thus, the fraction of sections sampled was 30/100 = 0.30. The number of neurons in the analysed region was estimated by multiplying the number of neurons counted within the sample regions by the reciprocals of the area sampling fraction and the fraction of section sampled.

Immunofluorescence

Animals were perfused and sections of 30 µm thickness were evaluated. Incubations and washes for all the antibodies were in PBS, pH 7.4. All work was done at RT. The slides were washed three times in PBS and then incubated with citrate 0,024% for 30 min at 80º C. After three washes, the slides were incubated with PBS-T 1% for 1 h. Then the sections were blocked with BSA (5%) in PBS-T 1% for 2 h. For double-labelling of TH with CASP3, the slides were incubated overnight at 4º C with either sheep-derived anti-TH (1:1000, NOVUS, NB300-110) and goat-derived anti-CASP3 (1:250, Cell signalling Technology, #9662S), diluted in PBS-T 1% containing 1% BSA. Thereafter, sections were washed six 10-min rinses in PBS-T 0.1%, and incubated with donkey anti-sheep secondary antibody conjugated to Alexa 647 (1:500, for TH; Thermo Fisher Scientific, A-21448) and rabbit anti-goat secondary antibody conjugated to Alexa 488 (1:500, for CASP3; Thermo Fisher Scientific, A11055), diluted in PBS-T 0.1% containing 1% BSA, for 1 h at 22 ± 1º C in the dark. Thereafter, sections were washed six 10-min rinses in PBS-T 0.1% and mounting with 50 % glycerol. In parallel, we carried out the respective negative controls to verify the specificity of the antibodies (data not shown). Fluorescence images were acquired using a confocal laser scanning microscope (Zeiss LSM 7 DUO) and processed using Fiji ImageJ (W. Rasband, National Institutes of Health).

Real-Time RT-PCR

Animals used for RT-PCR were sacrificed by decapitation. SN was dissected from each mouse, snap frozen in liquid nitrogen and stored at -80° C. Total RNA was extracted from the mouse SN of different groups using RNeasy® kit (Qiagen). cDNA was synthesized from 1 µg of total RNA using Revert Aid First Strand cDNA Synthesis Kit (Thermo Fisher Scientific) in 20 µL reaction volume as described by the manufacturer.

Real-time PCR was performed using 5 μL SensiFAST™ SYBR NO-ROX KIT (Bioline, United States), 0.4 μL of each primer, and 4.2 μL cDNA to get to a final reaction volume of 10 μL for 384-well plate. Controls were carried out without cDNA. Amplification was run in a Lightcycler® 480 Instrument II (Roche) thermal cycler at 95° C for 2 min followed by 40 cycles consisting of a denaturation phase for 5 s at 95° C, followed by a second phase of hybridization at 65° C for 10 s, and a final phase of elongation at 72° C for 20 s. The process was terminated by a final step of 7 min at 72° C. Analysis confirmed a single PCR product. β-actin served as reference gene and was used for samples normalization. The cycle at which each sample crossed a fluorescence threshold (Ct value) was determined, and the triplicate values for each cDNA were averaged. The primer sequence are: TH (F:5´- GGCTATGCTCTCCCTCACG and R:5´- CTTCTCTTTGATGTCACGCACG) and β-actin (F:5´- CTGAAGGGCCTCTATGCTAC and R: 5´- CCACAGTACCGTTCCAGAAG)

Microdialysis

Microdialysis in the corpus striatum was performed with an I-shaped cannula (Santiago and Westerink, 1990). The exposed tip of the dialysis membrane was 2 mm. The dialysis tube (ID: 0.22 mm; OD: 0.31 mm) was prepared from polyacrylonitrile/sodium methalyl sulfonate copolymer (AN 69, Hospal, Barcelona, Spain). The stereotaxic coordinates used were AP = +0.4 mm; L = ±2.5 mm, DV = -1.0 mm (De Leonibus et al., 2005).

The perfusion experiments were carried out at 24 h and at 48 h after implantation of the probe. Microdialysis and subsequent chemical analysis were performed using an automated on-line sample injection system (Westerink et al., 1987). The corpus striatum was perfused at a flow rate of 3.0 μl/min, using a microperfusion pump (model 22, Harvard Apparatus, South Natick, MA, U.S.A.), with a Ringer's solution containing (in mM): NaCl, 140; KCl, 4.0; $CaCl_2$, 1.2; and $MgCl_2$, 1.0. With the help of an electronic timer, the injection valve was held in the load position for 15 min, during which the sample loop (40 μl) was filled with dialysate. The valve then switched automatically to the injection position for 15 s. This procedure was repeated every 15 min, the time needed to record a complete chromatogram.

Electron microscopy

Two control and two TH-CASP3KO mice were deeply anesthetized with pentobarbital (80 mg/kg i.p.) and perfused intracardially for 5 min with ice-cold 4% paraformaldehyde, 0.1% glutaraldehyde and 0.02% Ca Cl_2 in 0.12 M phosphate buffer, pH 7.3 (PB) fixative, followed by ice-cold 4% paraformaldehyde and 0.02% Cl_2Ca in PB fixative for 20 min. After dissection, the brains were stored overnight in the last fixative at 4º C. Coronal sections (50 μm thick) of the brain were cut on a Leica 1000S vibratome and collected in PBS. After incubation in PBS and

0.025% Triton X100 (10 min RT), the sections were immersed for 1 h in blocking solution (10% BSA in PBS) and incubated overnight with a rabbit polyclonal anti-TH antibody (1:500, Sigma, T8700) diluted in a solution of 5% BSA in PBS without Triton X100. After several rinses in PBS, the sections were incubated for 1 h in donkey anti-rabbit biotinylated IgG (1:200, Invitrogen, A16039) diluted in PBS. Thereafter, the sections were incubated for 1 h in ABC (Vector) diluted 1:400 in PBS. The conjugate was revealed by 0.3% DAB and 0.04% nickel sulphate in PB. After several rinses in PB, the labelling in the caudate nucleus was checked and selected labelled sections were postfixed in 1% osmium tetroxide in 0.1 M cacodylate buffer (pH 7.2), stained in block with 1% uranyl acetate in 70% ethanol, dehydrated with an increased gradient of ethanol, and embedded in Durcupan (Fluka®). Semithin (1.5 µm) and ultrathin (60-70 nm) sections were obtained on a Leica UC6 ultramicrotome. Semithin sections were stained with 1% toluidine blue. Ultrathin sections were collected in copper grids (150 and 300 mesh), and observed without counterstaining in a Zeiss Libra EM at 80 kV (CITIUS, University of Seville).

For quantitative analysis mosaics of the dorsal caudate nucleus of 3 x 3 (85 μm^2 area) microphotographs were obtained with the multiple image acquisition application of the Olympus iTEM software®. Mosaics of a same section were stitched by using the Image Composite Editor software (Microsoft®), obtaining images whose area ranged between 233.53 and 614.13 μm^2. To ensure that all synapses considered for counting were absolutely different, each mosaic series were obtained from ultrathin sections ribbons collected on grids whose cutting distance was of 3 µm far from the precedent grid. All counting were made with the Fiji ImageJ software (W. Rasband, National Institutes of Health).

Data analyses and statistics

Data were analysed with GraphPad PrismTM 4.0 (GraphPad Software, San Diego, CA, USA). Results are expressed as mean ± SEM values. Data were analyzed by using unpaired Student's t-test or repeated measures ANOVA (post-hoc Newman-Keuls). The level of significance was set to $p<0.05$.

RESULTS

$TH^{Cre}CASP3^{f/-}$ conditional mice.

To study the role of CASP3 in dopaminergic neurons, a conditional mouse was generated with CASP3 depletion in those neurons (see Material and Methods section and Fig. 1A). Next, we wondered if our experimental mice effectively had a specific reduction of CASP3 expression in TH-positive neurons. For that, we performed immunofluorescence assays to detect CASP3 in TH-positive neurons. Staining was generally mild with cytoplasmic and nuclear location, as it

has been previously described in human and canine neurons, and in human lymphocytes (Ramuz et al., 2003; Schlein et al., 2019). The intensity of CASP3 labelling observed presented a significant reduction of ~62% ($p=0.002$) in the mean intensity of CASP3 in TH-positive neurons in the SN pars compacta (SNpc) of the experimental mice in comparison with the control ones (Fig. 1B, C).

CASP3 deletion in TH neurons alters dopaminergic system in TH-CASP3KO mice.

In order to estimate the number of TH-positive neurons in the SNpc in TH-CASP3KO and control mice (Fig. 2A, B and C), an immunohistochemistry approach was used. This analysis demonstrated a more intense TH immunohistochemical signal in the SNpc of TH-CASP3KO mice than in controls (Fig. 2A and B). Indeed, optical density of TH immunoreactivity in SNpc (Fig. 2D; $p<0.01$) and VTA (Suppl. Fig. 1B; $p<0.01$) were increased as compared with controls. To corroborate the increase in TH immunostaining in the midbrain, the level of TH mRNA was measured by qPCR obtaining an increase of ~41% in the TH-CASP3KO *vs*. control animals (Fig. 2E; $p<0.01$). We next performed a stereological analysis of TH-positive neurons in the entire SN and found a significant increase by 1.5 times in the number of TH-positive neurons in TH-CASP3KO animals (Fig. 2B; $p<0.05$). Further support of a developmental deficit in the midbrain relies on the volume of the SNpc, which increased by ~54% in TH-CASP3KO mice ($p<0.01$; Fig. 2C). Other catecholaminergic nuclei, such as the locus coeruleus, were studied, but no differences were found between the experimental groups (Suppl. Fig. 1).

The striatum is the main target of dopaminergic innervation arising from the neurons of the SNpc; for that, we wondered if the increase of TH-positive neurons in SNpc led to the increase in dopaminergic projection fibres to the striatum. Surprisingly, a ~15% decrease of TH-immunoreactivity was found in TH-CASP3KO mice (Fig. 2F, G; $p<0.05$).

***In vivo* levels of dopamine and its metabolites are altered in TH-CASP3KO mice.**

Microdialysis was performed in the striatum of control and experimental mice to measure both extracellular basal levels of DA and its metabolites (3,4-Dihydroxyphenylacetic acid (DOPAC) and homovanillic acid (HVA)) and potassium-induced release. This analysis demonstrated a reduction in the striatal basal levels of DA (~58%; Fig. 3A; $p<0.05$) and HVA (~44%; Fig. 3C; $p<0.05$) in TH-CASP3KO animals compared with controls. Furthermore, the extracellular output of DA augmented in both groups after the perfusion of KCl 60 mM aimed to depolarize neurons and evoke DA release (Fig. 3D), although DA level remained lower in the striatum of TH-CASP3KO mice than in control ones.

***Casp3* deletion in TH neurons alters the number of synapses in the caudate nucleus of TH-CASP3KO mice.**

According with the complexity of their postsynaptic elements, chemical central nervous system synapses have been classified into four main types from the simplest ones, in which the active zone faces a straight postsynaptic density, to the more complex ones, such as those formed by mossy fibres (for a review, (Petralia et al., 2018)). Here, two main groups of synapses have been considered: (i) axospinous synapses (Fig. 4A-C, s), and non-axospinous synapses including both axodendritic and axosomatic synapses (Fig. 4A-B, arrows). From pioneer descriptions, the dopaminergic nigrostriatal synapses were mainly simple synapses: 59% axospinous; 35% axodendritic; 6% axosomatic (for a review, (Smith and Bolam, 1990)). These descriptions have been confirmed here in striatal TH-immunolabelled synapses observed by electron microscopy (Fig. 4D-E, asterisks). Quantification of all synapses (labelled and unlabelled ones) did not show significant differences between TH-CASP3KO and control mice in neither the number of striatum synapses (Fig. 4I, T; $p=0.31$) nor their ratio according the size of the striatum neuropile used for counts (control 1608.09 μm^2 mean = 321.62 ± 42.58 μm^2 *vs.* TH-CASP3KO 1589.47 μm^2 mean = 397.37 ± 73.60 μm^2; $p=0.41$) (Fig. 4G, T; $p=0.23$). However, significant differences were found in the types of synapses between the experimental groups in the dorsal caudate nuclei. Thus, an increase in the number of non-axospinous synapses (Fig. 4I-J, nAS; $p<0.05$) accompanied by a clear decrease in the number of type 1 or perforated synapses (Fig. 4I-J, P; $p<0.05$) was consistently found in the caudate nucleus of TH-CASP3KO mice relative to the controls. Since significant differences were found in striatal TH optical density between control and TH-CASP3KO mice (Fig. 2F-G), we considered quantifying both, TH-immunolabelled synapses and TH-immunolabelled profiles throughout the dorsal caudate neuropil (Fig. 4D-E, lp). In the caudate nucleus of TH-CASP3KO animals, the number of labelled presynaptic terminals (Fig. 4G, $p<0.05$), the number of TH labelled profiles (Fig. 4F, $p<0.05$), and the ratio of TH labelled presynaptic endings (Fig. 4H, $p<0.05$) were lower than in the controls. Taken together, these data reinforce the observation that TH-CASP3KO mice show lower TH innervation in the dorsal caudate nucleus than the control ones. This decrease was accompanied by a misbalanced distribution of plastic synapses (i.e. type 1 or perforated synapses; (Petralia et al., 2018)), whose number was lower in TH-CASP3KO mice.

TH-CASP3KO mice exhibit hypolocomotion, repetitive and perseverative behaviours.

In the striatum of TH-CASP3KO mice, less TH^+ synapsis and reduced DA release may indicate that this model could have motor behaviour impairment. To test this, a complete set of behaviour paradigms was carried out. Strong male bias in ASD prevalence has been consistently observed (consensus ratio of ~4:1 (male/female)) (Werling and Geschwind, 2013). Consequently, males were used to avoid confounding effects ascribed to female sex hormones. First, spontaneous locomotor activity was reduced in TH-CASP3KO mice compared with the control animals (Fig. 5A; ~30% of the control mice; $p<0.01$). This reduction was also observed

after amphetamine administration (Suppl. Fig. 2); interestingly, activity did not decrease over time in comparison with control mice (Fig. 5B). Therefore, TH-CASP3KO mice did not show any habituation to the context. Resting time in the experimental group, as it was expected after locomotor activity results, was increased ~72% (Fig. 5C; $p<0.05$). Second, using the same test, the typical stereotypies in mice were measured, founding and increase in both grooming and rearing movements in TH-CASP3KO mice compared with the control group (Fig. 5D). Next, we wondered if these motor alterations were accompanied by impairment of motor coordination and balance. The rotarod performance of TH-CASP3KO mice was similar to the control group in both the accelerated rotarod (4 to 40 rpm; Fig. 5E) and constant velocity during the trial 2 and 3 (5 rpm; Fig. 5F). However, we have found a temporal improvement in the rotarod performance during the trial 1 in TH-CASP3KO mice (see Fig. 5F). Despite this, both experimental groups had a progressive decrease in the number of falls compared with the first trial (Fig. 5F; $p<0.001$). Therefore, decreased activity along with increased of stereotypes in our model could also be linked to anxiety- and/or depression-like behaviour. To study this, the time spent in the margin of the open field arena in comparison with the centre was measured; the time spent in the margin was ~51% higher in TH-CASP3KO than in control mice (Fig. 6A, B; $p<0.01$). Furthermore, the experimental mice showed a thrice increment of fecal boluses in open field test (Fig. 6C; $p<0.001$). Another typical test to measure anxious behaviour is the buried marble test (Fig. 6D); in this test, experimental mice buried less marbles than controls (Fig. 6E; $p<0.01$). Additionally, after performance of the tail suspension test (Fig. 6F), TH-CASP3KO mice showed more immobility ($p<0.001$) and clasping ($p<0.01$), and less swinging ($p<0.001$) than control mice (Fig. 6G). Taken together, these data indicated that TH-CASP3KO mice exhibited hypolocomotor activity and altered behaviour associated with typical anxiety- and depression-like behaviour.

TH-CASP3KO mice display atypical responses to sensory stimuli.

Repetitive behaviour could be related to sensorimotor gating deficit (Perry et al., 2007). In order to test this, the acoustic startle response (ASR) and PPI ratio were measured in control and TH-CASP3KO mice. PPI measures the attenuation of a reflexive startle response when starting stimulus is delivered after a weak pre-stimulus (prepulse). Significant differences at different decibel levels were detected at low intensities pulses (prepulses intensities) in TH-CASP3KO mice (Fig. 7A). However, they did not show differences in auditory startle response to a 120 dB broadband noise pulse (Fig. 7B) or in PPI (when prepulses were delivered at intensities of 3 dB, 6 dB, and 12 dB above a background noise of 65 dB) in comparison with control mice (Fig. 7C). Furthermore, TH-CASP3KO displayed higher latency to uncover buried food in the olfactory test (Fig. 7D; $p<0.01$) and a decreased thermal threshold, indicated by lower response

latency in hot plate (Fig. 7E; $p<0.001$). These results may represent evidence of a "sensory modulation behaviour" in reaction to aversive sensory experience in the TH-CASP3KO mice.

TH-CASP3KO mice exhibit a reduced social interaction and nesting ability.

Mus musculus are a highly social species. Therefore, after the results previously described, it was necessary to investigate social interaction in the experimental mice. First, a modified home cage was used to test social approach behaviour; the home cage contains a wirecage, empty or occupied for stranger mice from a different strain (Fig. 8A). TH-CASP3KO mice spent less time (~13% lower than the control group; Fig. 8B; $p<0.05$) in close proximity to the object (empty wirecage). This difference was greater (~41% less time) when the wirecage contained a stranger mouse (Fig. 8B; $p<0.001$). Similarly, the latency to first contact was higher in TH-CASP3KO mice than in control group when the compartment was empty (Control: 23.75 ± 3.3 s; TH-CASP3KO: 52.7 ± 4.5 s; $p<0.001$) and when it was occupied with a stranger mouse (Control: 8.6 ± 1.5 s; TH-CASP3KO: 66.5 ± 3.8 s; $p<0.001$; Fig. 8C). Finally, time spent sniffing the empty object or the stranger mouse (Fig. 8A) was longer in control mice (Fig. 8D; $p<0.001$). Second, the nesting patterns in the home cage were studied since changes could indicate impairment in social behaviour. Examples of nests built by control and TH-CASP3KO mice 1 h after introduction of nesting material into the cage are shown in Fig. 8E. The height (Fig. 8F) and quality score (Fig. 8G) of the nesting were reduced in TH-CASP3KO at 1 h, but recovered control mice level at 24 h (Fig 8F, G). Altogether, these results indicate that the absence of CASP3 in TH neurons triggered an altered behaviour, including clear social deficit behaviour.

DISCUSSION

We present strong evidence that selective deletion of the *Casp3* gene within TH-expressing cells impairs the normal developmental of midbrain dopaminergic neurons as evidenced by a significant increase in the number of dopaminergic neurons in SN and VTA along with significant higher volume of the ventral mesencephalon. These findings confirm the key role of CASP3 in shaping the midbrain to ensure proper dopaminergic synaptic connections as previously suggested (Jackson-Lewis et al., 2000; Janec and Burke, 1993). Neurochemical, anatomical and behavioural analysis of TH-CASP3KO demonstrated an overall dopaminergic hypofunction and a behavioural pattern resembling core symptoms of ASD. Our study revitalizes the importance of DA-associated pathways in the aetiology of ASD.

CASP3 is an executioner caspase known primarily for its role in apoptosis although there has been a growing identification of novel non-apoptotic functions ascribed to this caspase in the brain (Hyman and Yuan, 2012; Shen et al., 2018). Depending of the mouse strain, *Casp3*KO

mice may die perinatally along with hyperplasias and disorganized cell migration in the brain (Hyman and Yuan, 2012). Ventral midbrain dopaminergic neurons have been shown to die by apoptosis during early postnatal development even though the genesis of these neurons is complete during embryogenesis (Bayer et al., 1995). During this period, the co-existence of normal SNpc neurons with degenerating cells exhibiting morphological features of apoptosis along with CASP3 activation is evident (Jackson-Lewis et al., 2000). However, conclusive evidence supporting a critical role of CASP3 driving the developmental death of dopaminergic neurons is lacking. Consequently, the generation of conditional *Casp3*KO mice specific for catecholaminergic neurons arise as a prerequisite to test the direct involvement of this caspase in the development of mesencephalic dopaminergic neurons. In addition, and given the pleiotropic roles of DA in motor activity, motivation, attention and reward processing (Wise, 2004), any developmental impairment of the dopaminergic system may be useful to identify its potential involvement in psychiatric diseases. In order to validate our model, we first studied the state of the dopaminergic system in the different catecholaminergic nuclei. Using densitometry analysis, we found that TH-*Casp3*KO mice showed alterations in the SNpc, VTA, and striatum but not in locus coeruleus. Stereological analysis demonstrated an increase in the number of TH-positive neurons in the whole ventral mesencephalon along with larger volume of the ventral midbrain. These results were confirmed by the measurement of the mRNA levels of TH in the midbrain using qPCR. Our analysis fits well with the regionally-specific apoptotic death of nigral dopaminergic neurons during early postnatal development (Jackson-Lewis et al., 2000). Indeed, during this period, the selective death of nigral dopaminergic neurons sculpt the midbrain to clearly define the SNpc (Jackson-Lewis et al., 2000), a feature not entirely present in TH-CASP3KO mice. Taken together, our study supports the involvement of CASP3 in governing the fate of nigral dopaminergic neurons during the period of target competition for appropriate synapses

Since neuronal programmed cell death is inherently associated to innervating target tissues to select functional synapses (Dekkers et al., 2013), presynaptic dopaminergic function was analysed by combining microdialysis, immunohistochemistry and electron microscopy.

Densitometric analysis of TH-labelled dopaminergic terminals demonstrated significant less innervation in striatum, thus suggesting affectation of nigrostriatal circuit, which control key aspects of motor motivation (Wise, 2004). The presence of less TH-positive fibers in the striatum of TH-CASP3KO mice could be accompanied by a decline of DA release. Firing associated to striatal dopaminergic terminals will dictate DA release and its basal extracellular levels. Potassium-evoked DA release and DA basal extracellular levels were significantly reduced in TH-CASP3KO mice, a clear indication of dopaminergic hypofunction in dopaminergic innervating tissues. Further support of this view is deduced from extracellular

output of DOPAC and HVA in response to KCl perfusion. Altogether, these data suggest that the specific deletion of *Casp3* in TH neurons impairs the dopaminergic system that in turn is unable to maintain normal DA levels in the striatum.

It is well established that functional synapses are selected through competition of target-derived growth factors during brain development. Having established an important role of CASP3 in shaping the dopaminergic system in the midbrain leading to overall dopaminergic hypofunction, we next studied the architecture of striatal synapses by electron microscopy, which revealed numerous synaptic differences. The number of positive TH profiles, the TH ratio of positive synapses with respect to the total, and the ratio between TH positive synapses and the number of non-synaptic positive TH profiles were significantly lower in the TH-CASP3KO group. In contrast, no significant differences were found in the total number of synapses per area or in the total number of synapses counted between the two groups thus supporting that the synaptic decrease in the TH-CASP3KO group is exclusively due to the alteration of the dopaminergic pathways.

Once we demonstrated that our TH-CASP3KO mouse exhibited abnormalities in the dopaminergic pathways, we designed a battery of behavioural tests to analyse relevant functions ascribed to DA including motor activity, motivation and reward processing (Wise, 2004). Remarkably, our experimental mice exhibited impaired social interaction, restrictive interests and repetitive stereotypic behaviours (*e.g.* self-grooming), which are considered the core symptoms of ASD (Lai et al., 2014). Since our animal mouse model exhibits neurochemical dopaminergic deficits through a CASP3-dependent mechanism, it becomes plausible that alterations in the dopaminergic system play a significant role in the aetiology of ASD. Indeed, different lines of evidence from clinical studies have implicated DA deficits in ASD (Dichter et al., 2012b; Ernst et al., 1997; Lee et al., 2018; Pavăl, 2017; Scott-Van Zeeland et al., 2010). Further, the mesolimbic cortex and striatum have been both linked to ASD through a DA imbalance in those brain areas (Damasio and Maurer, 1978; Maurer and Damasio, 1982). In fact, it is interesting to note that transgenic mice affecting specific DA pathways have shown only a restrictive behavioural pattern resembling ASD. Thus, D1A KO mice show some repetitive behaviours, including self-grooming (Cromwell et al., 1998). Further, another hallmark of ASD is social avoidance, which has been associated to prefrontal cortex neurons projecting to medium spiny neurons expressing D2 receptors. In fact, it is not surprising that several authors have proposed a dopaminergic hypothesis to explain several features of ASD (Kuo and Liu, 2018; Pavăl, 2017). Yet, transgenic mouse models of DA deficiency that recapitulate all core symptoms of ASD have been elusive so far. Evidence supporting this hypothesis comes from the signalling alterations displayed in the mesolimbic and nigrostriatal dopaminergic pathways of autistic subjects (Chevallier et al., 2012; Ernst et al., 1997; Haber,

2014; Scott-Van Zeeland et al., 2010). The mesolimbic pathway is involved in high-order brain functions such as reward and motivation-related behaviours (Chevallier et al., 2012), and some studies have shown that ASD is characterized by a general hypoactivation of the reward system (Dichter et al., 2012b), which occurs for both social and non-social rewards (Dichter et al., 2012c; Scott-Van Zeeland et al., 2010). Supporting this view, DA release is reduced in areas related to the mesolimbic system (Ernst et al., 1997; Scott-Van Zeeland et al., 2010). In our experimental mice, loss of motivation was supported by the hypolocomotion and anxiety in the open field test and the decreased number of buried marble test (Thomas et al., 2009) while impairment of social behaviour was deduced from the social interaction and the nest construction tests. Indeed, animal models showing alterations in social behaviour have been proposed in the literature as models of ASD (Bielsky et al., 2004; Caston et al., 1998; Engelmann and Landgraf, 1994; Lijam et al., 1997; Schneider and Przewłocki, 2005; Wersinger et al., 2002).

The stereotyped behaviours observed in autistic patients have been suggested to arise from a dysfunction of the nigrostriatal pathway, which controls the motor aspects of goal-directed behaviour in order to develop appropriate actions towards obtaining a specific outcome (Chevallier et al., 2012; Haber, 2014). In fact, our TH-CASP3KO mice showed ritual movements and motor stereotypes at much higher levels than control animals, in line with previously reported animal models of ASD (Caston et al., 1998; Hornig et al., 1999; Schneider and Przewłocki, 2005; Silverman et al., 2010; Wolterink et al., 2001). Another interesting feature present in a high percentage of ASD patients, especially children, is sensory abnormalities (Kern et al., 2006; Kohl et al., 2014; Leekam et al., 2007; Tomchek and Dunn, 2007). Remarkably, our experimental mice also showed signs of a faster nociceptive reaction and a greater response to startle to acoustic stimuli, indicating a hypersensitivity to sensory stimuli (pain and hearing sensitivity). Our model also showed that TH-CASP3KO animals have higher latency to uncover buried food in the olfactory test. It is worthy to note that alterations in olfaction are observed in ASD (Rozenkrantz et al., 2015), although it could also be an early symptom in neurodegenerative diseases such as Alzheimer´s, Parkinson´s and Huntington´s diseases (Attems et al., 2014) and in depression (Yuan and Slotnick, 2014).

All this data led us to suggest that specific *Casp3* deletion in the dopaminergic system could be an encouraging ASD model. However, we cannot exclude other possibilities. Hence, all the behavioural impairments that seem to occur at the initial phase of each test could be a consequence of low effort-based motivation, a deficit in preference for spatial and social novelty or even reflect learning impairments. Another issue is the fact that autism and ADHD share several neurological pathways and symptoms (Bariselli et al., 2016; Gargaro et al., 2011;

Viggiano et al., 2002). With our results we cannot rule out its comorbidity in our TH-CASP3KO model.

CONCLUSION

In summary, we provide compelling evidence supporting a key role of CASP3 in the development and synaptic maturation of the mesencephalic dopaminergic system. Specific deletion of *Casp3* in catecholaminergic neurons leads to DA hypofunction affecting nigrostriatal dopaminergic pathway. These mice exhibited a robust phenotype displaying all core symptoms of ASD. Indeed, most available ASD models fail to address heterogeneity of the disease, mimicking a minimal part of the aetiology. Typical examples include genetic mutations already described for the disease (Bielsky et al., 2004; Moles et al., 2004; Winslow et al., 2000), exposure to risk factors (Pletnikov et al., 2002; Schneider and Przewłocki, 2005), or injuries in areas that are known to be affected in these patients (Bobée et al., 2000; Schneider and Koch, 2005; Wolterink et al., 2001). Our study revitalizes the potential involvement of dopaminergic transmission in ASD and provides an excellent animal tool to further shed light into ASD pathogenesis.

REFERENCES

Abrahams, B.S., Geschwind, D.H., 2008. Advances in autism genetics: on the threshold of a new neurobiology. Nat Rev Genet 9(5), 341-355.

Arndt, T.L., Stodgell, C.J., Rodier, P.M., 2005. The teratology of autism. Int J Dev Neurosci 23(2-3), 189-199.

Attems, J., Walker, L., Jellinger, K.A., 2014. Olfactory bulb involvement in neurodegenerative diseases. Acta Neuropathol 127(4), 459-475.

Bariselli, S., Tzanoulinou, S., Glangetas, C., Prévost-Solié, C., Pucci, L., Viguié, J., Bezzi, P., O'Connor, E.C., Georges, F., Lüscher, C., Bellone, C., 2016. SHANK3 controls maturation of social reward circuits in the VTA. Nat Neurosci 19(7), 926-934.

Bayer, S.A., Wills, K.V., Triarhou, L.C., Verina, T., Thomas, J.D., Ghetti, B., 1995. Selective vulnerability of late-generated dopaminergic neurons of the substantia nigra in weaver mutant mice. Proc Natl Acad Sci U S A 92(20), 9137-9140.

Berrocoso, E., Ikeda, K., Sora, I., Uhl, G.R., Sánchez-Blázquez, P., Mico, J.A., 2013. Active behaviours produced by antidepressants and opioids in the mouse tail suspension test. Int J Neuropsychopharmacol 16(1), 151-162.

Berrocoso, E., Mico, J.A., 2009. Role of serotonin 5-HT1A receptors in the antidepressant-like effect and the antinociceptive effect of venlafaxine in mice. Int J Neuropsychopharmacol 12(1), 61-71.

Bielsky, I.F., Hu, S.B., Szegda, K.L., Westphal, H., Young, L.J., 2004. Profound impairment in social recognition and reduction in anxiety-like behavior in vasopressin V1a receptor knockout mice. Neuropsychopharmacology 29(3), 483-493.

Bobée, S., Mariette, E., Tremblay-Leveau, H., Caston, J., 2000. Effects of early midline cerebellar lesion on cognitive and emotional functions in the rat. Behav Brain Res 112(1-2), 107-117.

Burguillos, M.A., Deierborg, T., Kavanagh, E., Persson, A., Hajji, N., Garcia-Quintanilla, A., Cano, J., Brundin, P., Englund, E., Venero, J.L., Joseph, B., 2011. Caspase signalling controls microglia activation and neurotoxicity. Nature 472(7343), 319-324.
Caston, J., Yon, E., Mellier, D., Godfrey, H.P., Delhaye-bouchaud, N., Mariani, J., 1998. An animal model of autism: behavioural studies in the GS guinea-pig. Eur J Neurosci 10(8), 2677-2684.
Chevallier, C., Kohls, G., Troiani, V., Brodkin, E.S., Schultz, R.T., 2012. The social motivation theory of autism. Trends Cogn Sci 16(4), 231-239.
Cromwell, H.C., Berridge, K.C., Drago, J., Levine, M.S., 1998. Action sequencing is impaired in D1A-deficient mutant mice. Eur J Neurosci 10(7), 2426-2432.
Damasio, A.R., Maurer, R.G., 1978. A neurological model for childhood autism. Arch Neurol 35(12), 777-786.
De Leonibus, E., Oliverio, A., Mele, A., 2005. A study on the role of the dorsal striatum and the nucleus accumbens in allocentric and egocentric spatial memory consolidation. Learn Mem 12(5), 491-503.
Dekkers, M.P., Nikoletopoulou, V., Barde, Y.A., 2013. Cell biology in neuroscience: Death of developing neurons: new insights and implications for connectivity. J Cell Biol 203(3), 385-393.
Dichter, G.S., Damiano, C.A., Allen, J.A., 2012a. Reward circuitry dysfunction in psychiatric and neurodevelopmental disorders and genetic syndromes: animal models and clinical findings. J Neurodev Disord 4(1), 19.
Dichter, G.S., Felder, J.N., Green, S.R., Rittenberg, A.M., Sasson, N.J., Bodfish, J.W., 2012b. Reward circuitry function in autism spectrum disorders. Soc Cogn Affect Neurosci 7(2), 160-172.
Dichter, G.S., Richey, J.A., Rittenberg, A.M., Sabatino, A., Bodfish, J.W., 2012c. Reward circuitry function in autism during face anticipation and outcomes. J Autism Dev Disord 42(2), 147-160.
Elsabbagh, M., Divan, G., Koh, Y.J., Kim, Y.S., Kauchali, S., Marcín, C., Montiel-Nava, C., Patel, V., Paula, C.S., Wang, C., Yasamy, M.T., Fombonne, E., 2012. Global prevalence of autism and other pervasive developmental disorders. Autism Res 5(3), 160-179.
Engelmann, M., Landgraf, R., 1994. Microdialysis administration of vasopressin into the septum improves social recognition in Brattleboro rats. Physiol Behav 55(1), 145-149.
Ernst, M., Zametkin, A.J., Matochik, J.A., Pascualvaca, D., Cohen, R.M., 1997. Low medial prefrontal dopaminergic activity in autistic children. Lancet 350(9078), 638.
Franklin, K.a.P., G, 2019. Paxinos and Franklin's the Mouse Brain in Stereotaxic Coordinates, Compact. Academic Press.
Gargaro, B.A., Rinehart, N.J., Bradshaw, J.L., Tonge, B.J., Sheppard, D.M., 2011. Autism and ADHD: how far have we come in the comorbidity debate? Neurosci Biobehav Rev 35(5), 1081-1088.
Gundersen, H.J., Bagger, P., Bendtsen, T.F., Evans, S.M., Korbo, L., Marcussen, N., Møller, A., Nielsen, K., Nyengaard, J.R., Pakkenberg, B., 1988. The new stereological tools: disector, fractionator, nucleator and point sampled intercepts and their use in pathological research and diagnosis. APMIS 96(10), 857-881.
Haber, S.N., 2014. The place of dopamine in the cortico-basal ganglia circuit. Neuroscience 282, 248-257.
Hornig, M., Weissenböck, H., Horscroft, N., Lipkin, W.I., 1999. An infection-based model of neurodevelopmental damage. Proc Natl Acad Sci U S A 96(21), 12102-12107.
Hyman, B.T., Yuan, J., 2012. Apoptotic and non-apoptotic roles of caspases in neuronal physiology and pathophysiology. Nat Rev Neurosci 13(6), 395-406.
Jackson-Lewis, V., Vila, M., Djaldetti, R., Guegan, C., Liberatore, G., Liu, J., O'Malley, K.L., Burke, R.E., Przedborski, S., 2000. Developmental cell death in dopaminergic neurons of the substantia nigra of mice. J Comp Neurol 424(3), 476-488.
Janec, E., Burke, R.E., 1993. Naturally Occurring Cell Death during Postnatal Development of the Substantia Nigra Pars Compacta of Rat. Mol Cell Neurosci 4(1), 30-35.

Jeon, B.S., Kholodilov, N.G., Oo, T.F., Kim, S.Y., Tomaselli, K.J., Srinivasan, A., Stefanis, L., Burke, R.E., 1999. Activation of caspase-3 in developmental models of programmed cell death in neurons of the substantia nigra. J Neurochem 73(1), 322-333.
Kern, J.K., Trivedi, M.H., Garver, C.R., Grannemann, B.D., Andrews, A.A., Savla, J.S., Johnson, D.G., Mehta, J.A., Schroeder, J.L., 2006. The pattern of sensory processing abnormalities in autism. Autism 10(5), 480-494.
Kim, Y.S., Leventhal, B.L., Koh, Y.J., Fombonne, E., Laska, E., Lim, E.C., Cheon, K.A., Kim, S.J., Kim, Y.K., Lee, H., Song, D.H., Grinker, R.R., 2011. Prevalence of autism spectrum disorders in a total population sample. Am J Psychiatry 168(9), 904-912.
Kohl, S., Wolters, C., Gruendler, T.O., Vogeley, K., Klosterkötter, J., Kuhn, J., 2014. Prepulse inhibition of the acoustic startle reflex in high functioning autism. PLoS One 9(3), e92372.
Kuida, K., Zheng, T.S., Na, S., Kuan, C., Yang, D., Karasuyama, H., Rakic, P., Flavell, R.A., 1996. Decreased apoptosis in the brain and premature lethality in CPP32-deficient mice. Nature 384(6607), 368-372.
Kuo, C.T., Zhu, S., Younger, S., Jan, L.Y., Jan, Y.N., 2006. Identification of E2/E3 ubiquitinating enzymes and caspase activity regulating Drosophila sensory neuron dendrite pruning. Neuron 51(3), 283-290.
Kuo, H.Y., Liu, F.C., 2018. Molecular Pathology and Pharmacological Treatment of Autism Spectrum Disorder-Like Phenotypes Using Rodent Models. Front Cell Neurosci 12, 422.
Lai, M.C., Lombardo, M.V., Baron-Cohen, S., 2014. Autism. Lancet 383(9920), 896-910.
Lake, C.R., Ziegler, M.G., Murphy, D.L., 1977. Increased norepinephrine levels and decreased dopamine-beta-hydroxylase activity in primary autism. Arch Gen Psychiatry 34(5), 553-556.
Lee, Y., Kim, H., Kim, J.E., Park, J.Y., Choi, J., Lee, J.E., Lee, E.H., Han, P.L., 2018. Excessive D1 Dopamine Receptor Activation in the Dorsal Striatum Promotes Autistic-Like Behaviors. Mol Neurobiol 55(7), 5658-5671.
Leekam, S.R., Nieto, C., Libby, S.J., Wing, L., Gould, J., 2007. Describing the sensory abnormalities of children and adults with autism. J Autism Dev Disord 37(5), 894-910.
Li, Z., Jo, J., Jia, J.M., Lo, S.C., Whitcomb, D.J., Jiao, S., Cho, K., Sheng, M., 2010. Caspase-3 activation via mitochondria is required for long-term depression and AMPA receptor internalization. Cell 141(5), 859-871.
Lijam, N., Paylor, R., McDonald, M.P., Crawley, J.N., Deng, C.X., Herrup, K., Stevens, K.E., Maccaferri, G., McBain, C.J., Sussman, D.J., Wynshaw-Boris, A., 1997. Social interaction and sensorimotor gating abnormalities in mice lacking Dvl1. Cell 90(5), 895-905.
Lindeberg, J., Usoskin, D., Bengtsson, H., Gustafsson, A., Kylberg, A., Söderström, S., Ebendal, T., 2004. Transgenic expression of Cre recombinase from the tyrosine hydroxylase locus. Genesis 40(2), 67-73.
Maurer, R.G., Damasio, A.R., 1982. Childhood autism from the point of view of behavioral neurology. J Autism Dev Disord 12(2), 195-205.
Moles, A., Kieffer, B.L., D'Amato, F.R., 2004. Deficit in attachment behavior in mice lacking the mu-opioid receptor gene. Science 304(5679), 1983-1986.
Moretti, P., Bouwknecht, J.A., Teague, R., Paylor, R., Zoghbi, H.Y., 2005. Abnormalities of social interactions and home-cage behavior in a mouse model of Rett syndrome. Hum Mol Genet 14(2), 205-220.
Moy, S.S., Nadler, J.J., Young, N.B., Perez, A., Holloway, L.P., Barbaro, R.P., Barbaro, J.R., Wilson, L.M., Threadgill, D.W., Lauder, J.M., Magnuson, T.R., Crawley, J.N., 2007. Mouse behavioral tasks relevant to autism: phenotypes of 10 inbred strains. Behav Brain Res 176(1), 4-20.
Nóbrega, C., Nascimento-Ferreira, I., Onofre, I., Albuquerque, D., Hirai, H., Déglon, N., de Almeida, L.P., 2013. Silencing mutant ataxin-3 rescues motor deficits and neuropathology in Machado-Joseph disease transgenic mice. PLoS One 8(1), e52396.
Pavăl, D., 2017. A Dopamine Hypothesis of Autism Spectrum Disorder. Dev Neurosci 39(5), 355-360.

Perry, W., Minassian, A., Lopez, B., Maron, L., Lincoln, A., 2007. Sensorimotor gating deficits in adults with autism. Biol Psychiatry 61(4), 482-486.
Petralia, R.S., Wang, Y.X., Mattson, M.P., Yao, P.J., 2018. Invaginating Structures in Mammalian Synapses. Front Synaptic Neurosci 10, 4.
Pletnikov, M.V., Moran, T.H., Carbone, K.M., 2002. Borna disease virus infection of the neonatal rat: developmental brain injury model of autism spectrum disorders. Front Biosci 7, d593-607.
Ramos-Rodriguez, J.J., Molina-Gil, S., Rey-Brea, R., Berrocoso, E., Garcia-Alloza, M., 2013. Specific serotonergic denervation affects tau pathology and cognition without altering senile plaques deposition in APP/PS1 mice. PLoS One 8(11), e79947.
Ramuz, O., Isnardon, D., Devilard, E., Charafe-Jauffret, E., Hassoun, J., Birg, F., Xerri, L., 2003. Constitutive nuclear localization and initial cytoplasmic apoptotic activation of endogenous caspase-3 evidenced by confocal microscopy. Int J Exp Pathol 84(2), 75-81.
Rozenkrantz, L., Zachor, D., Heller, I., Plotkin, A., Weissbrod, A., Snitz, K., Secundo, L., Sobel, N., 2015. A Mechanistic Link between Olfaction and Autism Spectrum Disorder. Curr Biol 25(14), 1904-1910.
Santiago, M., Westerink, B.H., 1990. Characterization of the in vivo release of dopamine as recorded by different types of intracerebral microdialysis probes. Naunyn Schmiedebergs Arch Pharmacol 342(4), 407-414.
Schlein, L.J., Fadl-Alla, B., Pondenis, H.C., Lezmi, S., Eberhart, C.G., LeBlanc, A.K., Dickinson, P.J., Hergenrother, P.J., Fan, T.M., 2019. Immunohistochemical Characterization of Procaspase-3 Overexpression as a Druggable Target With PAC-1, a Procaspase-3 Activator, in Canine and Human Brain Cancers. Front Oncol 9, 96.
Schneider, M., Koch, M., 2005. Deficient social and play behavior in juvenile and adult rats after neonatal cortical lesion: effects of chronic pubertal cannabinoid treatment. Neuropsychopharmacology 30(5), 944-957.
Schneider, T., Przewłocki, R., 2005. Behavioral alterations in rats prenatally exposed to valproic acid: animal model of autism. Neuropsychopharmacology 30(1), 80-89.
Scott-Van Zeeland, A.A., Dapretto, M., Ghahremani, D.G., Poldrack, R.A., Bookheimer, S.Y., 2010. Reward processing in autism. Autism Res 3(2), 53-67.
Shen, X., Venero, J.L., Joseph, B., Burguillos, M.A., 2018. Caspases orchestrate microglia instrumental functions. Prog Neurobiol 171, 50-71.
Silverman, J.L., Yang, M., Lord, C., Crawley, J.N., 2010. Behavioural phenotyping assays for mouse models of autism. Nat Rev Neurosci 11(7), 490-502.
Smith, A.D., Bolam, J.P., 1990. The neural network of the basal ganglia as revealed by the study of synaptic connections of identified neurones. Trends Neurosci 13(7), 259-265.
Thomas, A., Burant, A., Bui, N., Graham, D., Yuva-Paylor, L.A., Paylor, R., 2009. Marble burying reflects a repetitive and perseverative behavior more than novelty-induced anxiety. Psychopharmacology (Berl) 204(2), 361-373.
Tomchek, S.D., Dunn, W., 2007. Sensory processing in children with and without autism: a comparative study using the short sensory profile. Am J Occup Ther 61(2), 190-200.
Urigüen, L., Gil-Pisa, I., Munarriz-Cuezva, E., Berrocoso, E., Pascau, J., Soto-Montenegro, M.L., Gutiérrez-Adán, A., Pintado, B., Madrigal, J.L., Castro, E., Sánchez-Blázquez, P., Ortega, J.E., Guerrero, M.J., Ferrer-Alcon, M., García-Sevilla, J.A., Micó, J.A., Desco, M., Leza, J.C., Pazos, A., Garzón, J., Meana, J.J., 2013. Behavioral, neurochemical and morphological changes induced by the overexpression of munc18-1a in brain of mice: relevance to schizophrenia. Transl Psychiatry 3, e221.
Vahia, V.N., 2013. Diagnostic and statistical manual of mental disorders 5: A quick glance. Indian J Psychiatry 55(3), 220-223.
Velmeshev, D., Schirmer, L., Jung, D., Haeussler, M., Perez, Y., Mayer, S., Bhaduri, A., Goyal, N., Rowitch, D.H., Kriegstein, A.R., 2019. Single-cell genomics identifies cell type-specific molecular changes in autism. Science 364(6441), 685-689.

Viggiano, D., Grammatikopoulos, G., Sadile, A.G., 2002. A morphometric evidence for a hyperfunctioning mesolimbic system in an animal model of ADHD. Behav Brain Res 130(1-2), 181-189.
Werling, D.M., Geschwind, D.H., 2013. Understanding sex bias in autism spectrum disorder. Proc Natl Acad Sci U S A 110(13), 4868-4869.
Wersinger, S.R., Ginns, E.I., O'Carroll, A.M., Lolait, S.J., Young, W.S., 2002. Vasopressin V1b receptor knockout reduces aggressive behavior in male mice. Mol Psychiatry 7(9), 975-984.
Westerink, B.H., Damsma, G., Rollema, H., De Vries, J.B., Horn, A.S., 1987. Scope and limitations of in vivo brain dialysis: a comparison of its application to various neurotransmitter systems. Life Sci 41(15), 1763-1776.
Westphal, D., Sytnyk, V., Schachner, M., Leshchyns'ka, I., 2010. Clustering of the neural cell adhesion molecule (NCAM) at the neuronal cell surface induces caspase-8- and -3-dependent changes of the spectrin meshwork required for NCAM-mediated neurite outgrowth. J Biol Chem 285(53), 42046-42057.
Williams, D.W., Kondo, S., Krzyzanowska, A., Hiromi, Y., Truman, J.W., 2006. Local caspase activity directs engulfment of dendrites during pruning. Nat Neurosci 9(10), 1234-1236.
Winslow, J.T., Hearn, E.F., Ferguson, J., Young, L.J., Matzuk, M.M., Insel, T.R., 2000. Infant vocalization, adult aggression, and fear behavior of an oxytocin null mutant mouse. Horm Behav 37(2), 145-155.
Wise, R.A., 2004. Dopamine, learning and motivation. Nat Rev Neurosci 5(6), 483-494.
Wolterink, G., Daenen, L.E., Dubbeldam, S., Gerrits, M.A., van Rijn, R., Kruse, C.G., Van Der Heijden, J.A., Van Ree, J.M., 2001. Early amygdala damage in the rat as a model for neurodevelopmental psychopathological disorders. Eur Neuropsychopharmacol 11(1), 51-59.
Wurzman, R., Forcelli, P.A., Griffey, C.J., Kromer, L.F., 2015. Repetitive grooming and sensorimotor abnormalities in an ephrin-A knockout model for Autism Spectrum Disorders. Behav Brain Res 278, 115-128.
Yuan, T.F., Slotnick, B.M., 2014. Roles of olfactory system dysfunction in depression. Prog Neuropsychopharmacol Biol Psychiatry 54, 26-30.
Zhang, J., Pho, V., Bonasera, S.J., Holtzman, J., Tang, A.T., Hellmuth, J., Tang, S., Janak, P.H., Tecott, L.H., Huang, E.J., 2007. Essential function of HIPK2 in TGFbeta-dependent survival of midbrain dopamine neurons. Nat Neurosci 10(1), 77-86.

ACKNOWLEDGEMENTS

This work was supported by grants from the Spanish Ministerio de Economía y Competitividad (SAF2015-64171-R and RTI2018-098645-B-I00). J.A.A. and E.P.V. was supported by a MINECO (BFU2015-64536) grant. I.S.P., E.B. and L.B. were co-financed by the "Fondo Europeo de Desarrollo Regional" (FEDER)-UE "A way to build Europe" from the "Ministerio de Ciencia, Innovación y Universidades" (RTI2018-099778-B-I00) and the "Ministerio de Salud-Instituto de Salud Carlos III (PI18/01691), as well as funding from the "Consejería de Salud de la Junta de Andalucía" (PI-0134-2018); the "Programa Operativo de Andalucía FEDER, Iniciativa Territorial Integrada ITI 2014-2020 Consejería Salud, Junta de Andalucía" (PI-0080-2017); the "Consejería de Economía, Innovación, Ciencia y Empleo de la Junta de Andalucía" (CTS-510); and the "Centro de Investigación Biomédica en Red de Salud Mental-CIBERSAM" (CB/07/09/0033). Images were obtained in the Centro de Investigación, Tecnología e Innovación de la Universidad de Sevilla (CITIUS).

FIGURE LEGENDS

Figure 1. Conditional TH-CASP3KO mice generation. (A) Crossing strategy for the generation of the TH-CASP3KO mice. (B) Coronal sections of SN of control and TH-CASP3KO animals showing immunoreactivity against CASP3 and TH; TH-CASP3KO mice lack CASP3 immunoreactivity (asterisks). (C) Quantification of CASP3 immunoreactivity in TH^+ cells. Data are expressed as mean ± SEM of n=3 mice/group. The two-tailed unpaired t test was used. **, $p<0.001$ *versus* control mice. Scale bar = 20 µm.

Figure 2: Effect of the deletion of *Casp3* on TH expression. (A) Coronal sections of SN from control and TH-CASP3KO animals showing immunoreactivity against TH. A greater immunoreactivity and number of fibres can be observed in the TH-CASP3KO animal. The deletion of *Casp3* generated differences in the percentage of TH-positive cells in the SN (B), volume of the SN in mm^3 (C), optical density of TH immunoreactivity (D) and TH mRNA expression level (E). Data are expressed as mean ± SEM of n=4 mice/group. The two-tailed unpaired t test was used. *, $p<0.05$, **, $p<0.01$ *versus* control mice. Scale bar = 250 and 100 µm. (F) Coronal sections from the Striatum of control and TH-CASP3KO animals showing immunoreactivity against TH. The deletion of *Casp3* decreased the optical density of TH immunoreactivity (G). Data are expressed as mean ± SEM of n=4 mice/group. The two-tailed unpaired t test was used. *, $p<0.05$ *versus* the control mice.

Figure 3. Effect of the deletion of *Casp3* on the levels of DA and its metabolites in the striatum. Quantification by microdialysis of DA (A) and its metabolites DOPAC (B) and HVA (D) in the striatum of control and TH-CASP3KO animals. Effect of 60 mM potassium perfusion on the extracellular levels of DA (D), DOPAC (E) and HVA (F) in the striatum of control and TH-CASP3KO animals. Data are expressed as mean ± SEM of n=4 mice/group. The two-tailed unpaired t test was used.*, $p<0.05$; ♯, $p<0.01$ *versus* control mice.

Figure 4. Synapses types in striatum. (A-E). Microphotographs from selected regions of the dorsal caudate nucleus illustrating the types of TH immunonegative (A-C) and immunopositive (D-E) synapses. Axosomatic (arrows in A and D) and axodendritic (B, arrow) synapses were considered together as non-axospinous synapses (nAS in I and J). Two types of axospinous synapses were considered; the most abundant was the macular synapse, whose presynaptic ending (A-C, asterisks) faces to a continuous postsynaptic density (A-C, s), while the less abundant perforated synapses have a small region of their postsynaptic region devoid of density invaginates (C, p, arrowheads) at the presynaptic ending (C, pr). TH labelled synapses (asterisk in D and E) were axosomatic (D, arrowhead) and axospinous (E), in which the postsynaptic density is even less evident (E, arrowheads) than in the same type of unstained synapses (E, s). (F-J) Quantification shows that the numbers of TH labelled profiles (F), the density of synapses

(G), the ratio between TH labelled synapses and TH non-synaptic labelled profiles (H), and the number of TH-labelled synapses (I, THl), are significantly lower in TH-CASP3KO caudate nucleus relative to the control ones. The significant decrease in the number of labelled (THl) (I and J) and perforated (P) (I and J) synapses, is correlated with a significant increase in the number of non axospinous (nAS) (I and J) and in the percentage of macular (M) (J) synapses in TH-CASP3KO caudate nucleus relative to the control ones. A two tailed Student's *t*-test was used to compare the data from TH-CASP3KO and control mice. Any p-value less than 0.05 was considered significant, indicated as follows: * $p<0.05$ and ** $p<0.01$. lp, TH non-synaptic labelled profile. n, neuron. s, spine. Bar = 1µm (A-E).

Figure 5. TH-CASP3KO mice are hypolocomotive and exhibit repetitive and perseverative behaviours. (A, B) TH-CASP3KO mice show a significantly reduced activity over 30 min (total activity; A) and for each time bin (every 5 min; B) in the open field test. Exploratory behaviour does not decrease over time in comparison with control mice (B). TH-CASP3KO mice do not show any habituation (B). TH-CASP3KO mice display an increased resting behaviour during the open field session (C), spending more time grooming and rearing than control animals (D). Their rotarod performance is comparable to control group, in both the accelerated rotarod (4 to 40 rpm; E) and constant velocity rotarod (5 rpm; F). Data are expressed as mean ± SEM of n=6-8 mice/group. The two-tailed unpaired t test was used (A, C-E). Repeated Measures ANOVA (post-hoc Newman-Keuls) was used (B, F).*, $p<0.05$; **, $p<0.01$; *** $p<0.001$ *versus* control mice. a.u.: arbitrary units.

Figure 6. TH-CASP3KO mice exhibit anxiety and depression-like behaviour. (A-C) TH-CASP3KO spend more time in the open field margins relative to the centre. (A) Representative traces of the open field activity and (B) its quantification, expressed as Log of the ratio of time spent in the margin and time in the centre (B). Additionally, the experimental group produced more fecal boluses during testing compared with control mice (C). (D, E) Representative images of marble burying TH-CASP3KO mice bury significantly fewer marbles over 30 min compared with the control group. (F) Photographs illustrating behaviour scores in the tail suspension test showing; immobility (mice hang without activity); swinging (keeping their body straight, continuously moving their paws in a vertical position and/or moving their bodies from side to side); curling (engaged in active twisting movements); and clasping (hind limb grasping behaviour towards the abdomen). TH-CASP3KO mice show more immobility and clasping and less active behaviours (swinging and curling) compared with control mice (G). Data are expressed as mean ± SEM of n=6-8 mice/group. The two-tailed unpaired t test was used.*, $p<0.05$; **, $p<0.01$; *** $p<0.001$ *versus* control mice.

Figure 7. TH-CASP3KO mice exhibit atypical responses to sensory stimuli. (A) Significant differences at all decibel levels were detected on acoustic startle responses to low intensities pulses in TH-CASP3KO mice. They showed no differences in either auditory startle response to a 120 dB broadband noise pulse (B) or in prepulse inhibition (PPI; when prepulses were delivered at intensities of 3 dB, 6 dB, and 12 dB above a background noise of 65 dB) in comparison with control mice (C). (D) TH-CASP3KO displayed higher latency to uncover buried food on olfactory test respect to control mice. (E) Increased response on hot plate in TH-CASP3KO measured as mean latency time to jump, lick or vocalize. Data are expressed as mean ± SEM of n=6-8 mice/group. The two-tailed unpaired t test was used. *, $p<0.05$: **, $p<0.01$; ***$p<0.001$ *versus* control mice.

Figure 8. TH-CASP3KO mice exhibit a reduced social interaction and nesting ability. (A) Diagram of a test box (home cage) containing a small compartment, which is either empty or occupied with stranger mice (from a different strain). (B) TH-CASP3KO mice spent less time in close proximity to the object (empty compartment) or the stranger mouse (time in chamber side), and more time away from it. Similarly, the latency to first contact (C) is higher than in control mice, and the duration of sniffing the object or the stranger mouse in control mice was longer in control mice (D). (E) Examples of nests built by control and TH-CASP3KO mice 1 h after the introduction of nesting material into the cage. The height (F) and quality score (G) of the nest was reduced in TH-CASP3KO mice at 1 h**,** but recovered the control level at 24 h. Data are expressed as mean ± SEM of n=6-8 mice/group. The two-tailed unpaired t test was used (B-D). Repeated Measures ANOVA (post-hoc Newman-Keuls) was used (F, G). *, $p<0.05$; **, $p<0.01$; ***, $p<0.001$ *versus* control mice. *** in red $p<0.001$ control *versus* control at 5 min. *** in blue $p<0.001$ TH-CASP3KO *versus* TH-CASP3KO at 5 min.

Supplementary Figure 1. **Effect of the deletion of *Casp3* on the expression of TH in dopaminergic and noradrenergic nuclei.** Optical density studies were performed in dopaminergic nuclei such as VTA (A, B), Locus coeruleus (C, D), and noradrenergic nuclei such as A7 (E, F), A5 (G, H), C1 (A4, I, J), A1 (K, L), A2 (M, N) and C2 and C3 (A3, O, P, Q) of control and TH-CASP3KO animals. No significant differences were found in the different nuclei except in the case of the VTA where an increase on the optical density of TH immunoreactivity in TH-CASP3KO mice was observed. Data are expressed as mean ± SEM of n=4 mice/group. The two-tailed unpaired t test was used. **, $p<0.01$ *versus* control mice.

Supplementary Figure 2. **TH-CASP3KO mice exhibited a slower response to amphetamine.** (A) Activity during amphetamine (Amph) injection in control (black square) and TH-CASP3KO (orange square) mice showing an enhanced locomotor activity following a single injection of 5 mg/kg i.p. of Amph. (B) Representative traces of locomotor activity in a

control and an experimental mouse. (C) Area generated in the graph representation of the activity during Amph administration in control (gray) and TH-CASP3KO (orange) mice. (D) Area under the curve in graph in C. Data are expressed as mean ± SEM of n=6-8 mice/group. The two-tailed unpaired t test was used (D).*, $p<0.05$; **, $p<0.01$ and ***, $p<0.001$ *versus* control mice. Repeated Measures ANOVA (post-hoc Newman-Keuls) was used (A). $^{+}$ in red $p<0.05$; $^{+++}$ in red $p<0.001$ control *versus* control at 5 min. $^{+}$ in blue $p<0.05$ TH-CASP3KO *versus* TH-CASP3KO at 5 min.

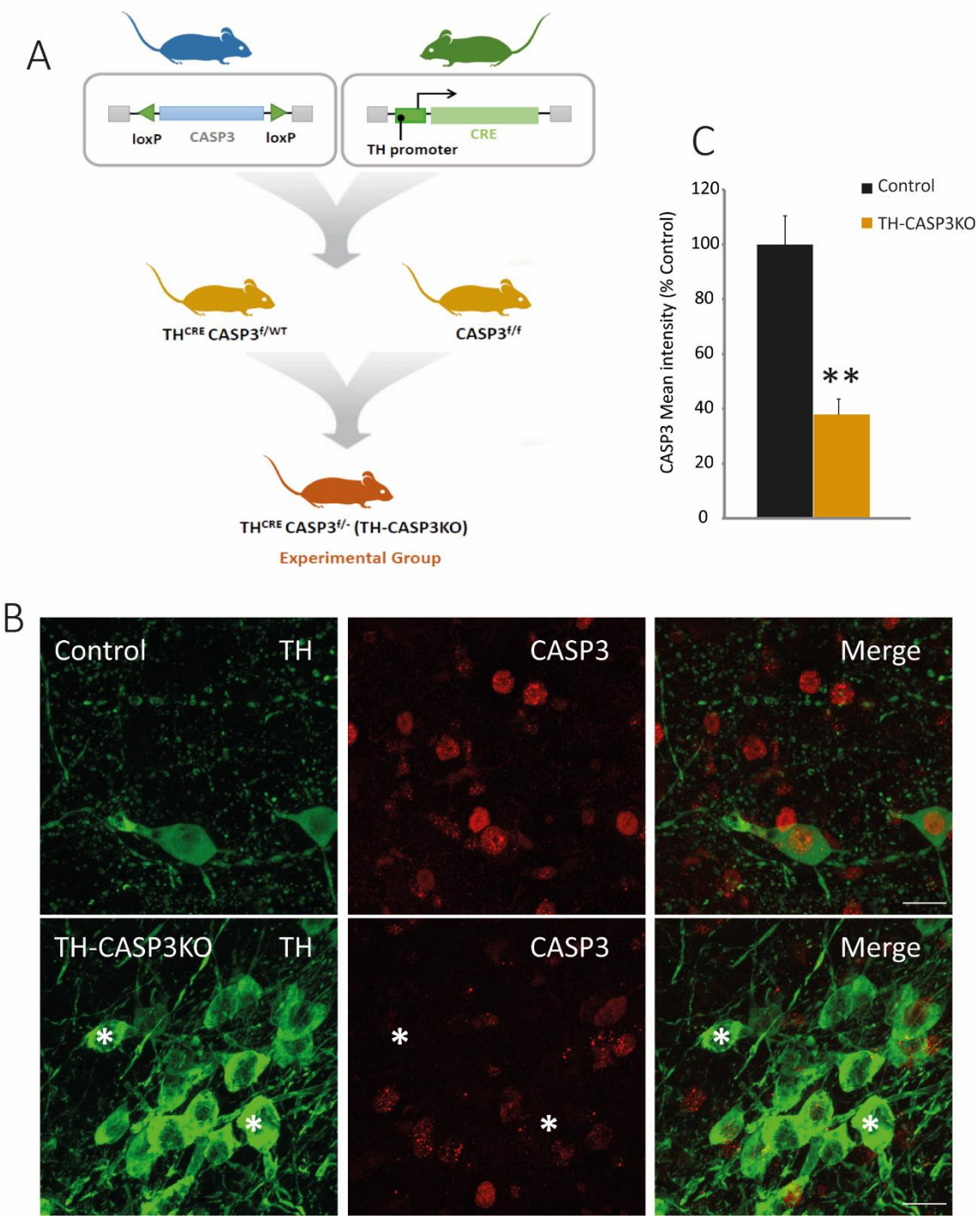
A
loxP
CASP3
loxP
CRE
TH promoter
THCRE CASP3f/WT
CASP3f/f
THCRE CASP3f/- (TH-CASP3KO)
Experimental Group
C
Control
TH-CASP3KO
CASP3 Mean intensity (% Control)
120
100
80
60
40
20
0
**
B
Control
TH
CASP3
Merge
TH-CASP3KO
TH
CASP3
Merge

Figure 1

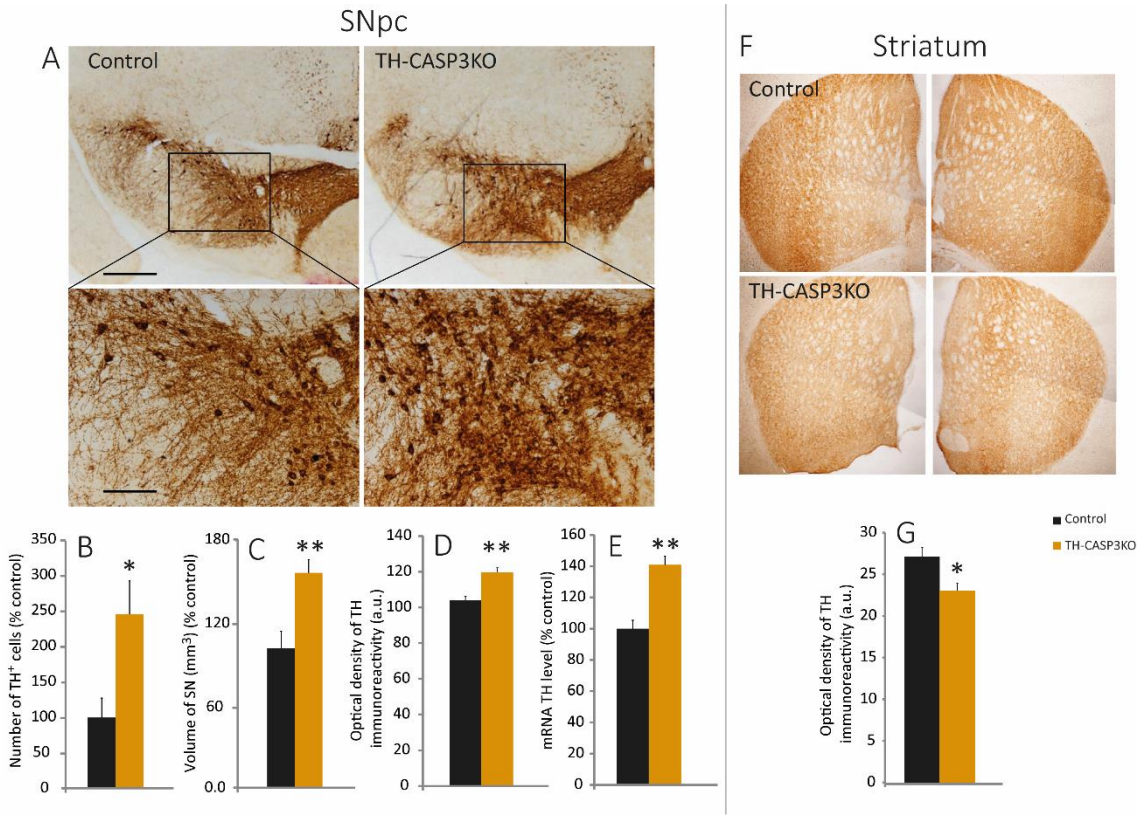

Figure 2

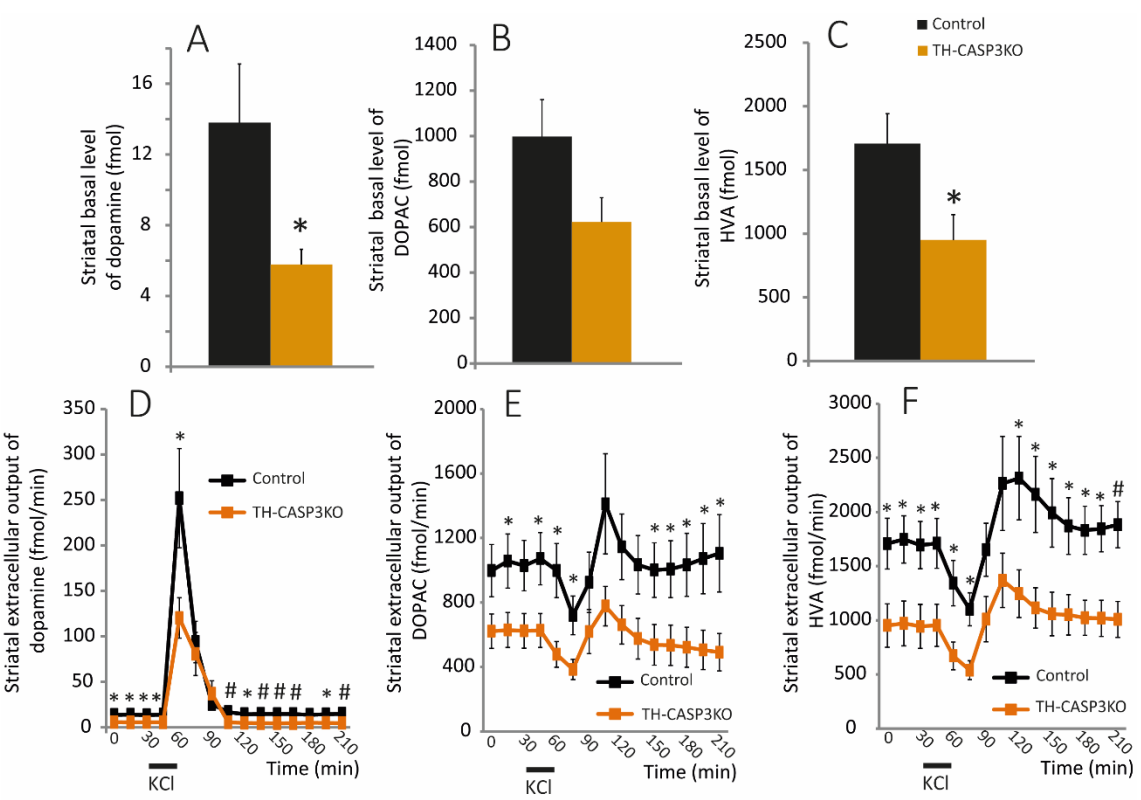

Figure 3

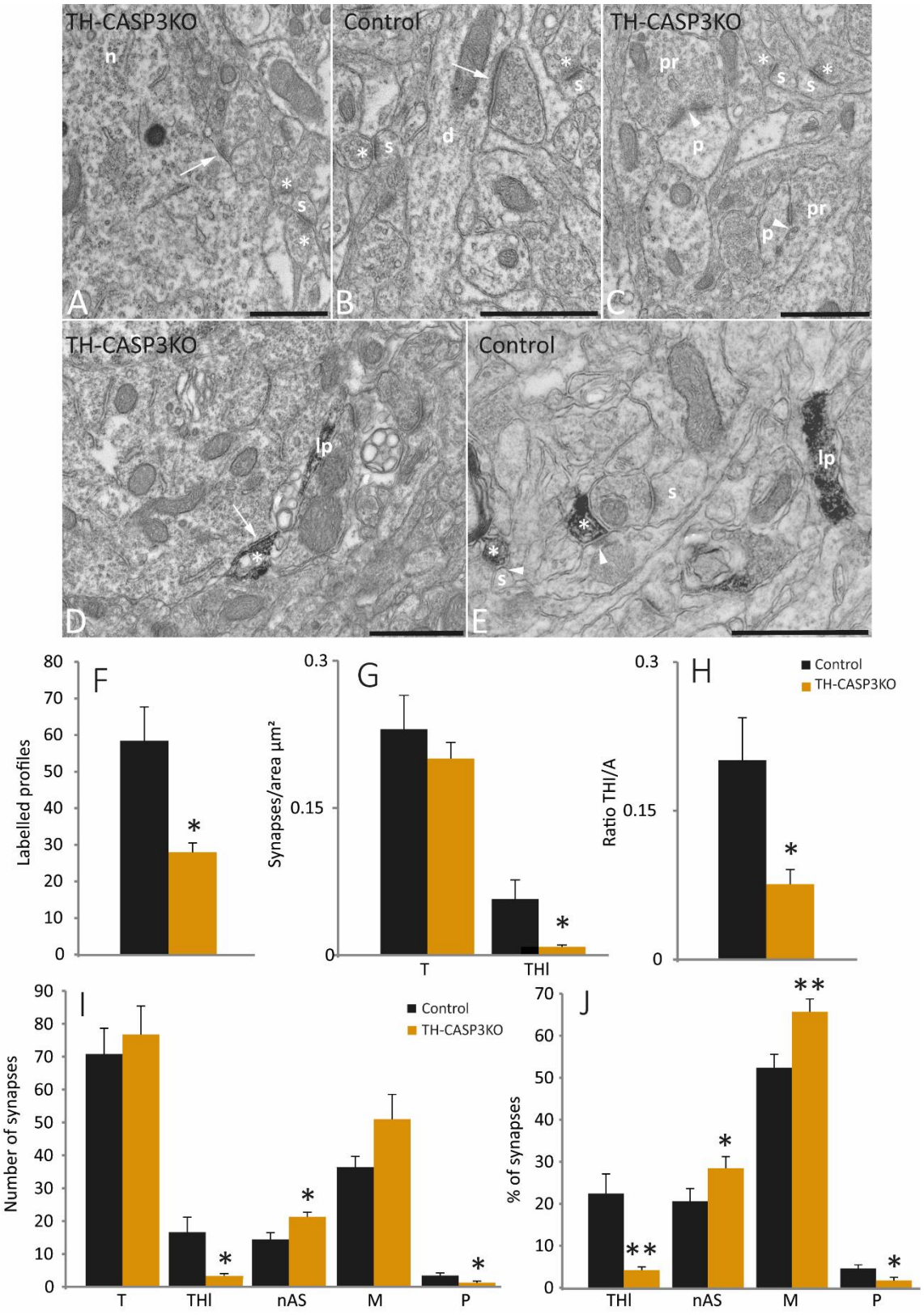
TH-CASP3KO
Control
TH-CASP3KO
n
s
d
pr
p
A
B
C
TH-CASP3KO
Control
lp
s
D
E
F
G
H
Labelled profiles
Synapses/area µm²
Ratio THI/A
Control
TH-CASP3KO
T
THI
I
J
Number of synapses
% of synapses
nAS
M
P

Figure 4

Figure 5

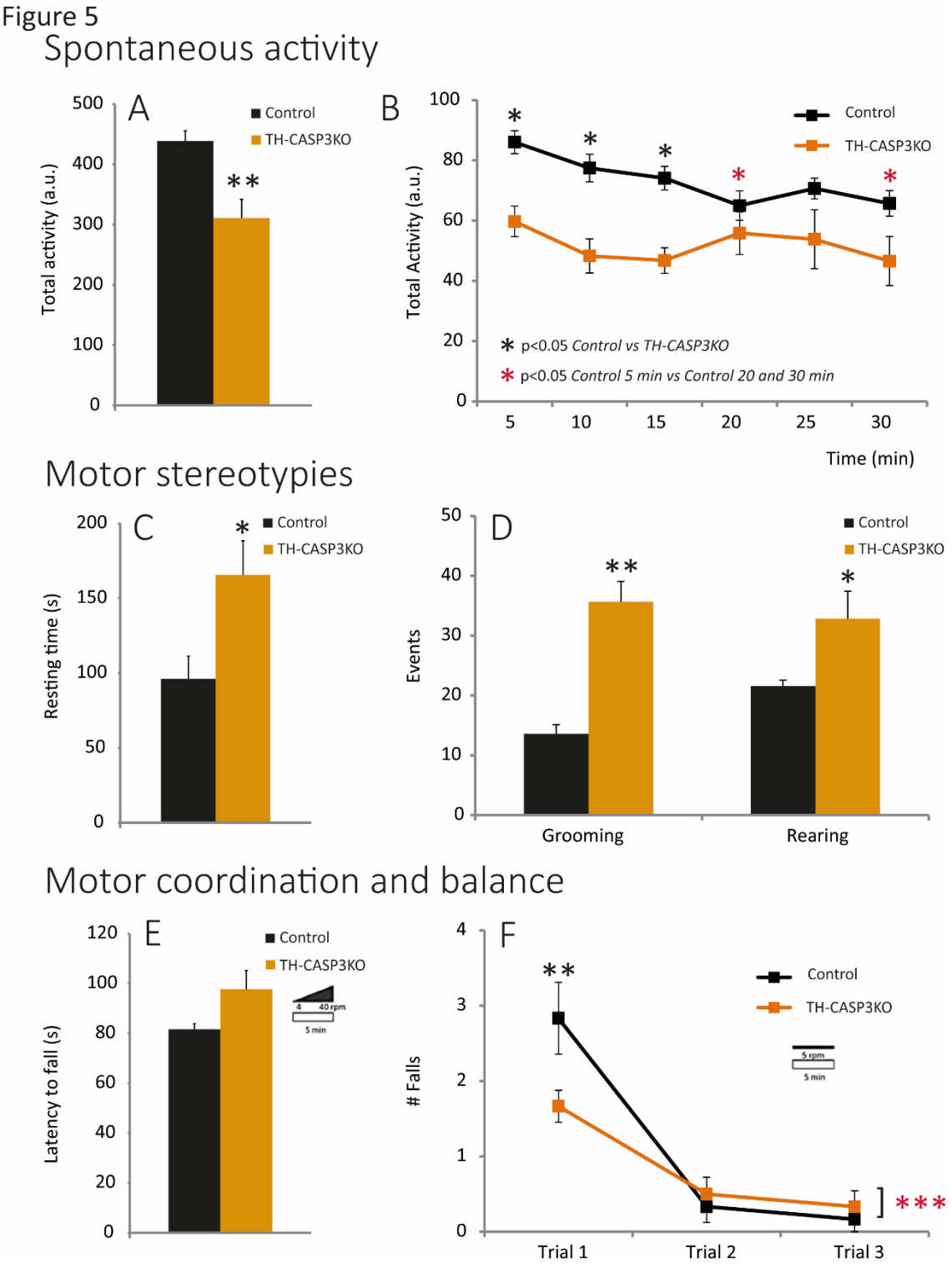
Spontaneous activity
A
Control
TH-CASP3KO
Total activity (a.u.)
500
400
300
200
100
0
**
B
Control
TH-CASP3KO
Total Activity (a.u.)
100
80
60
40
20
0
* p<0.05 Control vs TH-CASP3KO
* p<0.05 Control 5 min vs Control 20 and 30 min
5
10
15
20
25
30
Time (min)
Motor stereotypies
C
Control
TH-CASP3KO
Resting time (s)
200
150
100
50
0
*
D
Control
TH-CASP3KO
Events
50
40
30
20
10
0
**
*
Grooming
Rearing
Motor coordination and balance
E
Control
TH-CASP3KO
4
40 rpm
5 min
Latency to fall (s)
120
100
80
60
40
20
0
F
Control
TH-CASP3KO
5 rpm
5 min
Falls
4
3
2
1
0
**
***
Trial 1
Trial 2
Trial 3

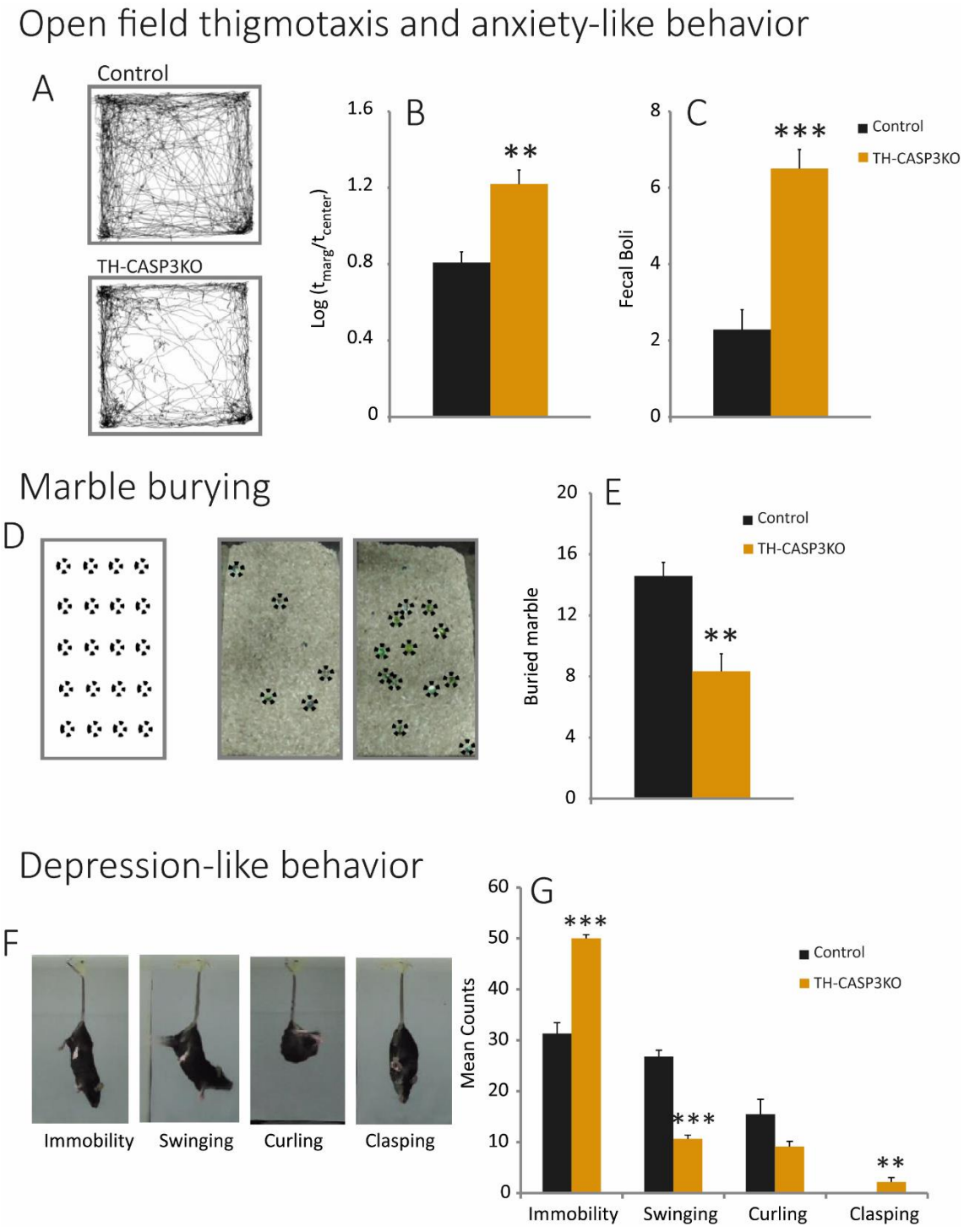
Open field thigmotaxis and anxiety-like behavior
A
Control
TH-CASP3KO
B
Log (t_{marg}/t_{center})
1.6
1.2
0.8
0.4
0
**
C
Fecal Boli
8
6
4
2
0
***
Control
TH-CASP3KO
Marble burying
D
E
Buried marble
20
16
12
8
4
0
**
Control
TH-CASP3KO
Depression-like behavior
F
Immobility
Swinging
Curling
Clasping
G
Mean Counts
60
50
40
30
20
10
0
***
***
**
Control
TH-CASP3KO
Immobility
Swinging
Curling
Clasping

Figure 6

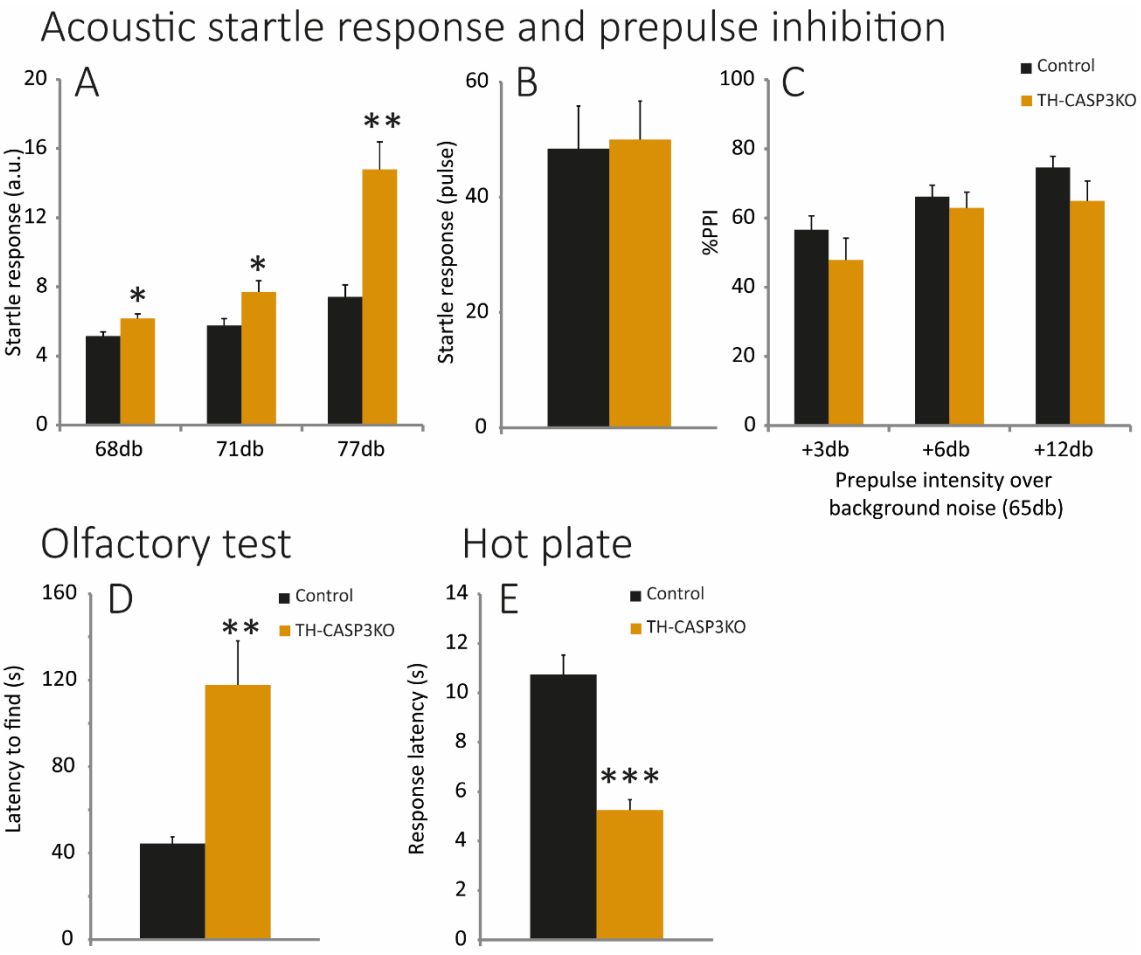
Acoustic startle response and prepulse inhibition
A
Startle response (a.u.)
68db
71db
77db
B
Startle response (pulse)
C
%PPI
Control
TH-CASP3KO
+3db
+6db
+12db
Prepulse intensity over background noise (65db)
Olfactory test
D
Latency to find (s)
Hot plate
E
Response latency (s)

Figure 7

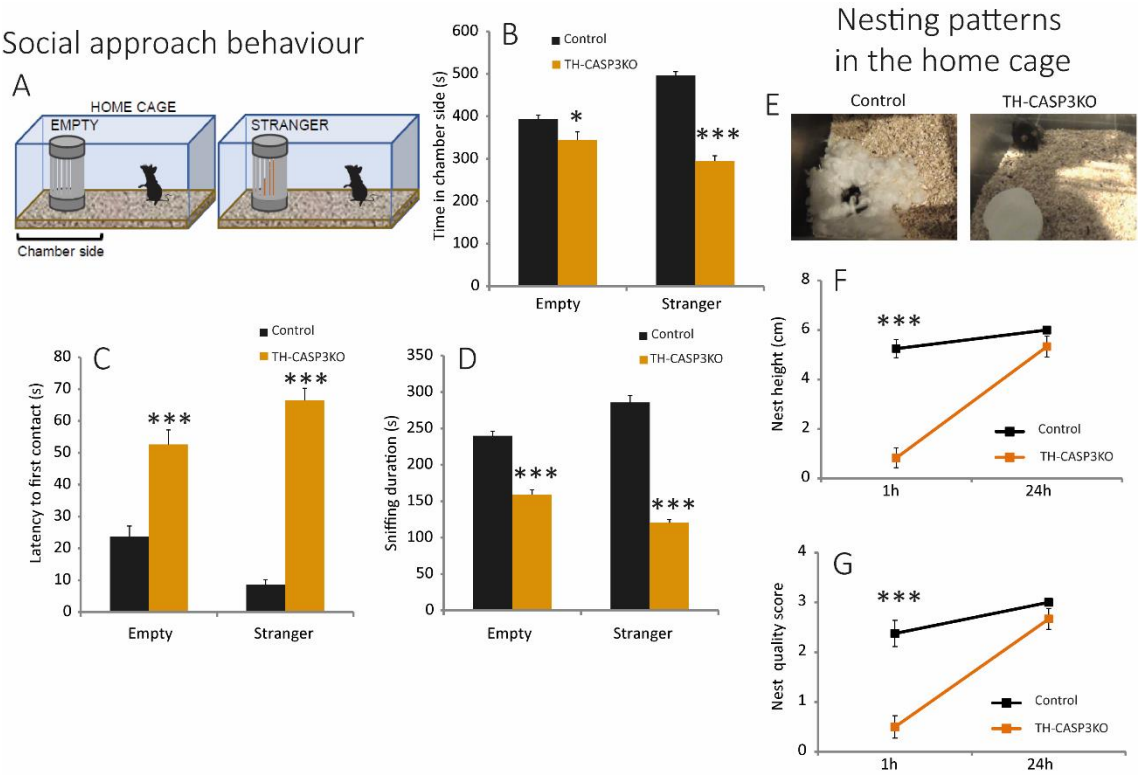
Social approach behaviour
A
HOME CAGE
EMPTY
STRANGER
Chamber side
B
Time in chamber side (s)
Empty
Stranger
C
Latency to first contact (s)
D
Sniffing duration (s)
Nesting patterns in the home cage
E
Control
TH-CASP3KO
F
Nest height (cm)
1h
24h
G
Nest quality score

Figure 8

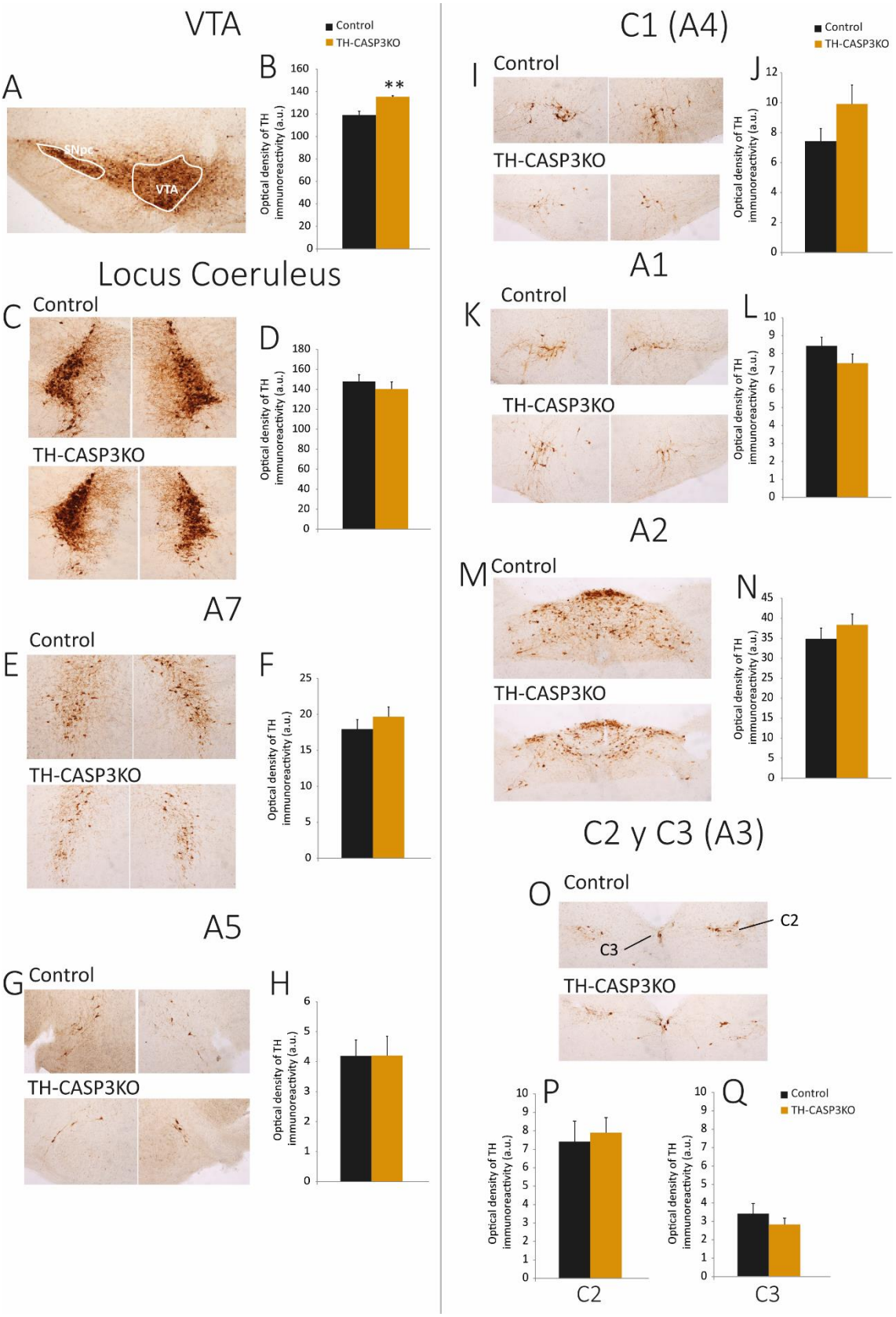

Supp. Figure 1

Supp. Figure 2

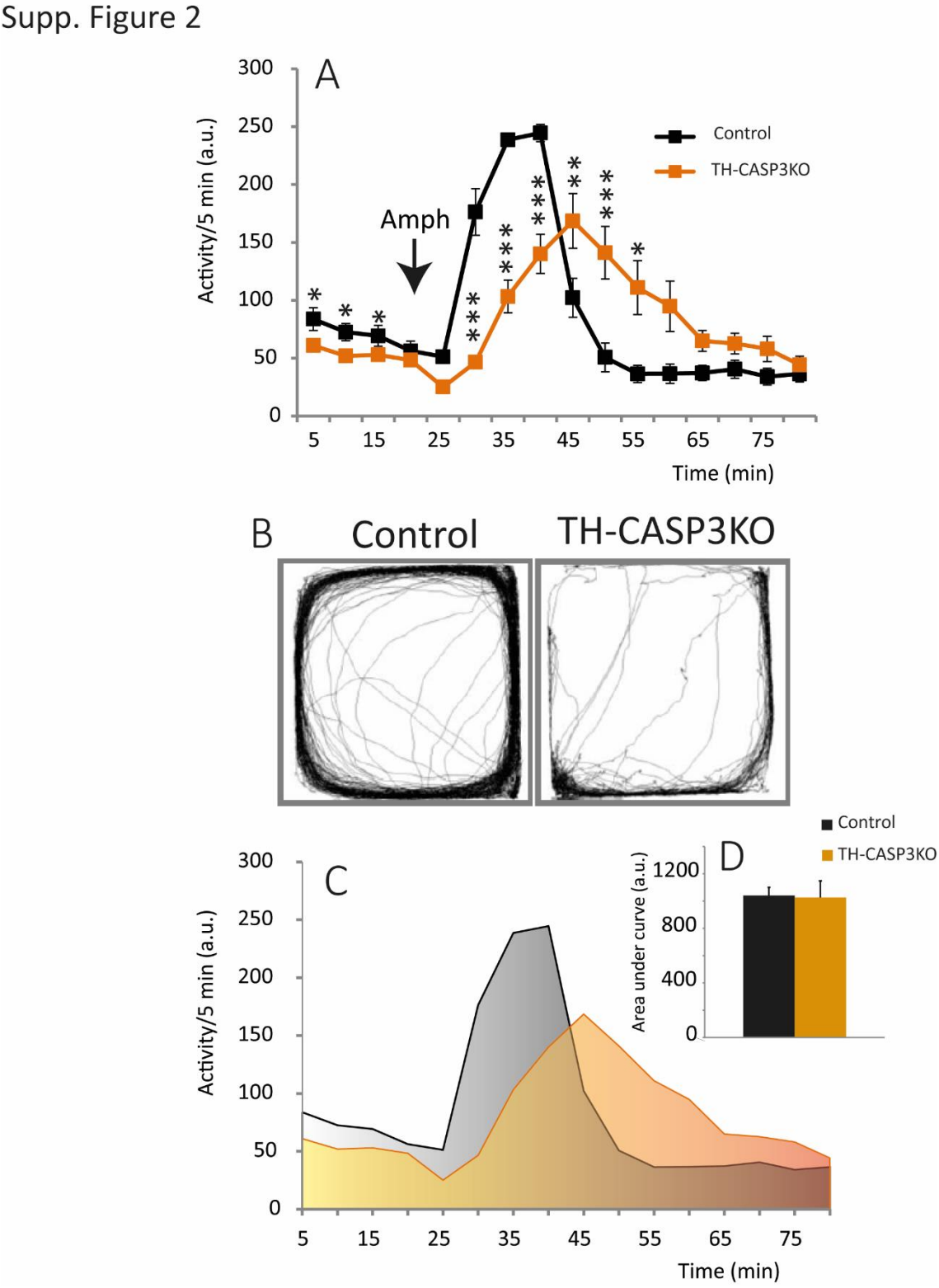

Supp. Figure 2